The blast pathogen effector AVR-Pik binds and stabilizes rice heavy metal-associated (HMA) proteins to co-opt their function in immunity

Oikawa, K. [1], Fujisaki, K.[1], Shimizu, M. [1], Takeda, T. [1], Saitoh, H. [1,2], Hirabuchi, A.[1], Hiraka, Y. [1], Białas, A.[3], Langner, T.[3], Kellner, R.[3], Bozkurt, T. O. [4], Cesari, S. [5], Kroj, T. [5], Maidment, J. H. R. [6], Banfield, M. J.[6], Kamoun, S.[3], Terauchi, R.[1,7]

[1] Iwate Biotechnology Research Center, Kitakami, Iwate, Japan

[2] Department of Molecular Microbiology, Tokyo University of Agriculture, Tokyo, Japan

[3] The Sainsbury Laboratory, University of East Anglia, Norwich Research Park, Norwich, NR4 7UH, UK

[4] Imperial College London, London, UK

[5] University of Montpellier, CIRAD, INRAE, Supagro, BGPI, Montpellier, France

[6] Department of Biological Chemistry, John Innes Centre, Norwich Research Park, Norwich, NR4 7UH, UK

[7] Laboratory of Crop Evolution, Kyoto University, Kyoto, Japan

Abstract

Plant intracellular nucleotide-binding domain and leucine-rich repeat-containing (NLR) immune receptors have a complex architecture. They can include noncanonical integrated domains that are thought to have evolved from host targets of pathogen effectors to serve as pathogen baits. However, the functions of host proteins with similarity to NLR integrated domains and the extent to which they are targeted by pathogen effectors remain largely unknown. Here, we show that the blast fungus effector AVR-Pik binds a subset of related rice proteins containing a heavy metal-associated (HMA) domain, one of the domains that has repeatedly integrated into plant NLR immune receptors. We find that AVR-Pik binding stabilizes the rice HMA proteins OsHIPP19 and OsHIPP20. Knockout of *OsHIPP20* causes enhanced disease resistance towards the blast pathogen, indicating that *OsHIPP20* is a susceptibility gene (*S*-gene). We propose that AVR-Pik has evolved to bind HMA domain proteins and co-opt their function to suppress immunity. Yet this binding carries a trade-off, it triggers immunity in plants carrying NLR receptors with integrated HMA domains.

Introduction

Plant pathogens target host proteins to promote disease by secreting effector proteins (Hogenhout et al. 2009). Some of these host targets have been co-opted by plant intracellular nucleotide-binding leucine rich repeat (NLR) immune receptors to act as baits to detect pathogens, and are then known as integrated domains (IDs) (Cesari et al. 2014; Wu et al. 2015; Sarris et al. 2016; Kroj et al. 2016). Genome-wide bioinformatics searches have found these domains in diverse immune receptors from multiple plant families (Sarris et al. 2016; Kroj et al. 2016; Baggs et al. 2017; Bailey et al., 2018). We hypothesize that such widespread NLR-IDs modulate basic immune responses that are conserved among plants. One such domain is the heavy metal-associated (HMA) domain found in four botanical families (Sarris et al. 2016). In rice, HMA domains have been integrated into two different NLRs, RGA5 (Okuyama et al. 2011) and Pik-1 (Ashikawa et al. 2008). In addition to rice (a member of Poaceae), HMA domains have also integrated into NLR immune receptors of plant species in the Brassicaceae, Fabaceae and Rosaceae (Sarris et al. 2016; Kroj et al. 2016). This indicates that HMA-containing proteins have probably been repeatedly targeted by pathogens across a diversity of flowering plants. Therefore, understanding the endogenous function of HMA-containing proteins has the potential to reveal important basic features of plant disease susceptibility and immunity. In this study, we identify rice HMA-containing proteins as targets of an effector of the blast pathogen *Magnaporthe* (syn. *Pyricularia*) *oryzae* and address their potential function.

The rice *Pik* locus comprises two NLR genes, *Pik-1* and *Pik-2*, and recognizes the *M. oryzae* effector AVR-Pik (Ashikawa et al. 2008). This recognition triggers plant immunity mediated by the hypersensitive response (HR). AVR-Pik is a 113-amino-acid protein originally defined as having no sequence similarity to known protein domains (Yoshida et al. 2009). More recently, structure-informed similarity searches showed that AVR-Pik belongs to the MAX (*Magnaporthe* AVRs and ToxB-like) family of fungal effectors (De Guillen et al. 2015), which adopt a six β-sandwich fold stabilized by buried hydrophobic residues, and commonly but not always, a disulphide bond. Pik-1 recognition of AVR-Pik is mediated by direct binding of the effector to an HMA domain (Maqbool et al. 2015) located between the N-terminal coiled-coil (CC) and nucleotide binding (NB) domains of Pik-1 (Kanzaki et al. 2012; Cesari et al., 2013). *AVR-Pik* and *Pik-1* are described as being involved in a coevolutionary arms race that has resulted in the emergence of allelic series of both effector genes in the pathogen and NLR genes in the host (Kanzaki et al. 2012; De la Concepcion et al. 2018; Białas et al. 2018).

Biochemical and structural analysis of complexes between AVR-Pik variants and HMA domains of different Pik-1 alleles revealed the molecular interactions between the effector and NLR-ID (Maqbool et al. 2015; De la Concepcion et al. 2018; De la Concepcion et al. 2019). This knowledge recently allowed structure-guided protein engineering to expand the recognition profile of a Pik NLR to different AVR-Pik variants (De la Concepcion et al. 2019). The Pik-1 HMA domains exhibit a four

β-sheets and two α-strands (βαββαβ) topology similar to the yeast copper transporter domain Ccc2A (Banci et al. 2001), even though the characteristic MxCxxC metal-binding motif is degenerate in Pik-1. The integrated HMA domain of RGA5 also adopts the classical HMA domain fold but, intriguingly, uses a different interface to interact with the *M. oryzae* effectors AVR-Pia and AVR1-CO39 (Guo et al. 2018).

HMA domains are also found in other plant proteins that are unrelated to NLRs (De Abreu-Neto et al. 2013). These proteins form large and complex families known as heavy metal-associated plant proteins (HPPs) and heavy metal-associated isoprenylated plant proteins (HIPPs), here collectively referred to as small proteins containing an HMA domain (abbreviated as sHMA proteins). One such sHMA protein is the product of the rice blast partial resistance gene *pi21* (Fukuoka et al. 2009). The recessive allele *pi21*, a presumed loss-of-function allele with a deletion mutation, confers partial broad-spectrum resistance to rice against compatible isolates of *M. oryzae.* This finding implicates HMA domain-containing proteins in rice defense (Fukuoka et al. 2009). However, the molecular function of Pi21 and other rice sHMA proteins have not been characterized to date.

Unlike other *M. oryzae* effectors, *AVR-Pik* does not show extensive presence/absence polymorphisms within the rice-infecting lineage, and its evolution in natural pathogen populations is mainly driven by nonsynonymous amino acid substitutions (Kanzaki et al. 2012; Shi et al. 2018). This suggests that *AVR-Pik* encodes an activity of benefit to the pathogen that is maintained in resistance-evading forms of the effector. To address the virulence function of AVR-Pik, we set out to identify rice proteins other than the Pik NLRs that interact with this effector. We found that AVR-Pik binds and stabilizes sHMA proteins. Knockout of one sHMA gene (*OsHIPP20*) conferred enhanced resistance to infection by the blast pathogen, suggesting *OsHIPP20* is a susceptibility gene (S-gene). Our model is that AVR-Pik effectors interfere with sHMA function by stabilizing these proteins to support pathogen invasion.

Results

AVR-PikD interacts with small heavy metal-associated proteins (sHMAs) of rice

To identify rice proteins that may be putative targets of AVR-PikD, we performed a yeast 2-hybrid screen (Y2H) with the effector as bait and a cDNA library prepared from leaves of rice cultivar Sasanishiki inoculated with *M. oryzae* as the prey. From this screen we identified four HMA-containing proteins, named OsHIPP19 (LOC_Os04g39350), OsHIPP20 (LOC_Os04g39010), OsHPP04 (LOC_Os02g37300) and OsHPP03 (LOC_Os02g37290) (De Abreu-Neto et al. 2013), as interactors of AVR-PikD, amongst other proteins (**Table S1**). The sizes of AVR-PikD interacting HMAs ranged from 118 (OsHPP03) to 123 (OsHIPP19) amino acids. Rice sHMA proteins typically comprise a conserved N-terminal HMA domain followed by a variable proline-rich domain (**Fig. 1**),

and may contain a C-terminal "CaaX" isoprenylation motif (where "a" represents an aliphatic amino acid and X represents any amino acid). They form a large protein family with 87 members in the rice genome (cultivar Nipponbare) as annotated by Rice Genome Annotation Project (Kawahara et al. 2013) (**Fig. 2**). Phylogenetic analyses of the aligned HMA domains of rice sHMA proteins revealed two clades supported by high bootstrap values (> 90%) with relatively large number of members that we designate here as Clades A and B. All four sHMA proteins interacting with AVR-PikD belong to Clade A (**Fig. 2**). Interestingly, the HMA domains of RGA5 and three alleles of the Pik-1 NLRs also cluster in Clade A. However, the integrated HMA domains of Pik-1 (Pik*-HMA, Pikm-HMA and Pikp-HMA) and RGA5 (RGA5-HMA) are on separate branches in the tree, indicating distinct lineages and diversification patterns.

To determine if AVR-PikD interacts with other Clade A sHMA proteins, we selected 9 that are expressed in rice leaves with FPKM (fragments per kilobase of exon per million reads mapped) value > 2 (**Fig. 2**) and tested pairwise interactions by Y2H (**Fig. 3**). This experiment showed that AVR-PikD binds around half of the tested Clade A sHMA proteins (**Fig. 2, 3, Fig S1**). We also tested binding of AVR-PikD with three sHMA proteins from Clade B, including OsHIPP05 (Pi21). These sHMA proteins did not bind AVR-PikD (**Fig. 2, 3, Fig S1**). These data reveal that AVR-PikD shows specific binding to Clade A sHMA proteins.

Further, we also tested the interaction of Clade A sHMA proteins OsHIPP19, OsHIPP20, OsHPP04, OsHPP03 and LOC_Os04g39380 with the *M. oryzae* effectors AVR-Pia and AVR1-CO39, which interact with the HMA domain of RGA5 (Cesari et al. 2013). We found that AVR-Pia and AVR1-CO39 did not bind any of the sHMAs tested (**Fig. S2**). Also, none of the three AVRs interacted with the Pi21 HMA protein (**Fig S2**).

Co-immunoprecipitation confirms AVR-PikD binding to OsHIPP19 and OsHIPP20

Interactions between AVR-PikD and OsHIPP19 and OsHIPP20 were further tested by co-immunoprecipitation using proteins expressed in *N. benthamiana* (**Fig. 4**). OsHIPP19 and OsHIPP20 were fused with a FLAG-epitope at their N-termini (FLAG:OsHIPP19 and FLAG:OsHIPP20), and AVR-PikD was tagged with the hemagglutinin (HA) epitope at the C-terminus (AVR-PikD:HA). These proteins were separately expressed in *N. benthamiana* leaves by *Agrobacterium tumefaciens* mediated transformation (agroinfiltration) and resulting leaf crude extracts were mixed and subjected to a pull-down experiment. Upon pull-down of FLAG:OsHIPP19 from leaf cell extracts with an anti-FLAG antibody, AVR-PikD was co-immunoprecipitated and detected following incubation with the anti-HA antibody (**Fig. 4**). A similar result was obtained for the interaction between OsHIPP20 and AVR-PikD. These results confirm that AVR-PikD binds OsHIPP19 and OsHIPP20 in plant extracts as well as in yeast.

All AVR-Pik variants tested bind rice sHMA proteins OsHIPP19 and OsHIPP20

Naturally occurring AVR-Pik variants are differentially recognized by allelic Pik NLRs. These recognition specificities correlate with the binding affinity of AVR-Pik variants to the integrated HMA domain of the Pik-1 NLR (Kanzaki et al. 2012; Maqbool et al. 2015; De la Concepcion et al. 2018; De la Concepcion et al., 2019). We tested whether the AVR-Pik variants AVR-PikA, C, or E, interact with the rice sHMA proteins OsHIPP19 and OsHIPP20 in Y2H. The results of this experiment (**Fig. 5, Fig. S3**) showed that similar to AVR-PikD, all AVR-Pik variants tested interacted with OsHIPP19 and OsHIPP20. This result suggests that all the tested AVR-Pik variants bind sHMAs, the possible host target proteins, whereas they vary in the recognition by different alleles of Pik NLRs.

AVR-PikD stabilizes OsHIPP19 and OsHIPP20 in plant cells

Next, we aimed to determine the effect of AVR-PikD binding to sHMA proteins. For this we co-expressed OsHIPP19 and OsHIPP20 with AVR-PikD in *N. benthamiana* leaves by agroinfiltration. Following expression, the leaf extract was separated into supernatant and pellet fractions by centrifugation, and each fraction was analyzed by western blot (**Fig. 6**). We used expression of GUS protein and AVR-Pii as controls that do not bind OsHIPP19 and OsHIPP20. In the supernatant fraction we observed that the OsHIPP19 and OsHIPP20 proteins were degraded to smaller fragments when co-expressed with GUS or AVR-Pii. However, when co-expressed with AVR-PikD, we detected stronger signals of intact molecules of OsHIPP19 and OsHIPP20. As an additional control we also tested OsHIPP17, an sHMA that does not bind AVR-PikD (**Fig. 2, 3, Fig. S4)**. We found that OsHIPP17 was degraded to a smaller fragment even in the presence of AVR-PikD. OsHIPP19 and OsHIPP20 proteins in the pellet fraction were not degraded irrespective of the presence or absence of AVR-PikD, whereas OsHIPP17 in the pellet was degraded to a smaller fragment. These results show that the AVR-PikD effector stabilizes sHMA proteins OsHIPP19 and OsHIPP20 in the plant cytosol, and this stabilization is specific to sHMA proteins that interact with this effector. We also noted a lower accumulation of AVR-PikD in the supernatant when co-expressed with OsHIPP17. This suggests the possibility that AVR-PikD may require interaction with other proteins in the plant cytosol for full stability.

AVR-PikD affects subcellular localization of OsHIPP19 and OsHIPP20 during co-expression in *N. benthamiana* leaves

After observing the enhanced stability of OsHIPP19 and OsHIPP20 on co-expression with AVR-PikD, we tested whether binding of AVR-PikD affected the subcellular localization of these sHMA proteins. For this, we transiently co-expressed GFP-tagged OsHIPP19 and OsHIPP20

(GFP:OsHIPP19 and GFP:OsHIPP20) in *N. benthamiana* leaves together with either GUS, AVR-Pii or AVR-PikD, and performed confocal microscopy. In the presence of GUS or AVR-Pii we found that GFP:OsHIPP19 and GFP:OsHIPP20 showed nucleo-cytoplasmic localization and accumulated in punctate structures with varying sizes (**Fig. 7**). Interestingly, when OsHIPP19 or OsHIPP20 was co-expressed with AVR-PikD, these punctae-like structures were not observed and the sHMA proteins were diffused in the cytoplasm and nucleus. This finding indicates that AVR-PikD binding alters the subcellular distribution of the sHMA proteins.

Knockout of the *OsHIPP20* gene reduces rice susceptibility to *Magnaporthe oryzae*

Of the seven sHMA proteins that interacted with AVR-PikD, we selected OsHIPP19, OsHIPP20 and OsHPP04 for further study because these were identified most frequently in the initial Y2H screen (**Table S1**) and showed strong interaction profiles with AVR-PikD (**Fig. 2, 3**). To explore the function of these sHMA proteins in rice, we generated knockout (KO) mutants by CRISPR/Cas9-mediated mutagenesis in the rice cultivar Sasanishiki (*Piks/Pia*), which is easy to transform and susceptible to the blast fungus isolate Sasa2 without *AVR-Pik* or *AVR-Pia*. We targeted *OsHIPP19* and *OsHPP04* genes individually, as well as *OsHIPP19* and *OsHIPP20* together (**Fig. 8, Fig. S5**). The resulting KO lines were challenged with the compatible *M. oryzae* isolate Sasa2. The *OsHIPP19* (two independent lines) and *OsHPP04* individual KO lines showed a similar level of infection as the wild-type control (Sasanishiki). However, the *OsHIPP20* KO line, as well as *OsHIPP19*+*OsHIPP20* double KO line, showed a reduction in lesion size caused by *M. oryzae* infection (**Fig. 8, Fig. S5**). These results indicate that *OsHIPP20* is a susceptibility (*S*-) gene that is required for full infection of rice (cultivar Sasanishiki) by *M. oryzae*.

Discussion

In this paper, we set out to identify the host targets of the *M. oryzae* effector AVR-Pik, and study the virulence function of this effector. We found that AVR-Pik binds multiple sHMA proteins of rice that belong to the same phylogenetic clade (Clade A), which also contains the integrated HMA of Pik-1 and RGA5 (**Fig 2, 3**). These findings support the view that NLR integrated domains have evolved from the host targets of pathogen effectors and that HMA-containing proteins are a major host target of plant pathogen effectors. In an independent study, Maidment et al. (2020) demonstrate that AVR-Pik binds to OsHIPP19 with nanomolar affinity *in vitro* and show the interaction of the effector with this sHMA is via an interface conserved with the Pik-1 integrated HMA domains providing further evidence that this effector targets host sHMA proteins.

Heavy metal-associated (HMA) domains were first defined in metal binding domains of P-type ATPase family copper transport proteins, including human MNK and WND proteins, mutations

of which cause Menkes disease and Wilson disease, respectively (Bull & Cox. 1994). HMA domains are also found in a number of heavy metal transport or detoxification proteins both in bacteria and eukaryotes. The yeast metallochaperone Atx1 was shown to deliver monovalent copper ions to the P-type ATPase Ccc2 that transports copper to trans-Golgi vesicle where it is taken up by the multicopper oxidase Fet3 (Askwith et al. 1994; Pufahl et al. 1997; Rosenzweig & O'Halloran. 2000). A typical HMA domain contains two conserved cysteine residues involved in metal binding in a MxCxxC motif that is located towards the N-termini of the domain (Bull & Cox, 1994).

In most organisms, only a small number of HMA-containing proteins have been reported. By contrast, in plants, proteins containing HMA-like domains have massively expanded (Dykema et al. 1999; Barth et al. 2009; De Abreu-Neto et al. 2013). For example, Barth et al. (2009) identified 44 Arabidopsis genes that encode for proteins containing an HMA domain and a C-terminal putative isoprenylation motif (CaaX). Based on the presence or absence of the C-terminal isoprenylation motif, De Abreu-Neto et al. (2013) grouped plant sHMAs into heavy metal-associated isoprenylated plant proteins (HIPPs) and heavy metal-associated plant proteins (HPPs). We have chosen to use the naming convention of De Abreu-Neto et al. (2013) here. In this manuscript, we present an analysis of the HMA-like repertoire of the rice (cultivar Nipponbare) genome, revealing the presence of at least 87 HMA-containing small protein (abbreviated as sHMA) genes (**Fig. 2**).

The biological functions of plant sHMA proteins reported so far are diverse. Two Arabidopsis HMA-containing proteins, CCH and ATX1, complemented yeast *atx1* mutant, and are presumed to be involved in copper transport (Himelbrau et al. 1998; Puig et al. 2007; Shin et al. 2012). Barth et al. (2009) showed that the Arabidopsis HMA-containing protein HIPP26 localizes to nuclei and interacts with a zinc-finger transcription factor ATHB29, while Gao et al. (2009) reported the same protein (with an alternative name, ATFP6) was localized to plasma membrane and interacted with acyl-CoA–binding protein ACBP2, which was hypothesized to be involved in membrane repair after oxidative stress. Zhu et al. (2016) reported that the Arabidopsis HMA-containing protein NaKR1 interacts with Flowering Locus T (FT) and mediates its translocation from leaves to shoot apices. Cowan et al. (2018) reported that potato mop-top virus (PMTV) movement protein TGB1 interacts with *Nicotiana benthamiana* sHMA protein HIPP26 and relocalizes this protein from the plasma membrane to the nucleus, thus contributing to PMTV long-distance movement by altering transcriptional regulation.

Genetic studies have also revealed roles of specific plant sHMA proteins in defense and susceptibility towards pathogens. Deletion in the proline-rich domain of Pi21, a rice sHMA, conferred a partial resistance against compatible isolates of *M. oryzae* (Fukuoka et al. 2009). Virus-induced gene silencing of wheat *TaHIPP1* enhanced resistance against stripe rust caused by *Puccinia striiformis* f. sp. *Triticii* (Zhag et al. 2015). Similarly, a knockout mutant of *Arabidopsis AtHMAD1* enhanced resistance against virulent *Pseudomonas syringae* DC3000 (Imran et al. 2016) and a knockout mutant of *Arabidopsis AtHIPP27* enhanced resistance against beet cyst nematode (Radakovic et al. 2018).

However, it remains unclear how these sHMA proteins impact interactions with these diverse pathogens. Nonetheless, given that HMA domains have integrated into NLR immune receptors in at least four botanical families, it is likely that HMA containing proteins have repeatedly been targeted by pathogens across a diversity of flowering plant species and are thus important components in plant-pathogen interactions.

In addition to Pik-1, the NLR RGA5 also carries an integrated HMA domain that binds two *M. oryzae* effectors, AVR-Pia and AVR1-CO39. However, in our Y2H assays with a high stringency conditions, we didn't detect any interaction between AVR-Pia and AVR1-CO39 and the tested sHMA proteins. We hypothesize that these two effectors may weakly bind the tested sHMAs or bind other rice sHMA proteins among the >80 members of this family.

In this study, we revealed that gene knockout of *OsHIPP20* confers enhanced resistance to rice against a compatible isolate of *M. oryzae* (**Fig. 8**). Therefore, like Pi21, OsHIPP20 is a susceptibility gene (*S*-gene), whose activity is required for full invasion of the *M. oryzae* pathogen in rice. We also found that AVR-PikD binds and stabilizes OsHIPP19 and OsHIPP20 (**Fig. 6**). We hypothesize that AVR-Pik–mediated stabilization of sHMA proteins suppresses host defenses, resulting in enhanced *M. oryzae* invasion of rice cells (**Fig. 9**). The next steps in this research are to determine the roles of the extended family of sHMA proteins in rice and other plants to understand the interplay between effector-mediated protein stabilization and disease.

Our conceptual and mechanistic understanding of how plant NLR proteins perceive pathogens continues to expand. In recent years, a novel model termed the integrated domain hypothesis has emerged and postulates that NLRs can bait pathogen effectors directly through integrated decoy/sensor domains (Cesari et al. 2014; Wu et al. 2015; Sarris et al. 2016; Kroj et al. 2016). These unconventional NLR domains are thought to have evolved by duplication and integration of an effector host target into the receptor protein. However, there are only very few examples where the evolutionary origin of the NLR integrated domain could be traced to an effector target (Le Roux et al. 2015; Sarris et al. 2015; Grund et al. 2020). Here, we show that AVR-Pik interacts with sHMA proteins that belong to the same phylogenetic clade as the HMA domains integrated into the rice NLRs Pik-1 and RGA5. Therefore, throughout evolution, the Pik-1 NLR immune receptor has co-opted sHMA proteins through the integration of an HMA domain and neofunctionalization of this domain as a bait for the effector (**Fig. 9**). This has launched a coevolutionary arms race between Pik-1 and AVR-Pik. Given that binding of AVR-Pik to Pik-1 HMA domains is necessary for triggering the hypersensitive response (HR) cell death and disease resistance in rice, new variants of AVR-Pik have arisen in *M. oryzae* populations that evade binding the integrated Pik-1 HMA but maintain their virulence activity (Kanzaki et al. 2012; Maqbool et al. 2015; Białas et al. 2018). Here we show that each of the AVR-Pik variants tested retain their binding to OsHIPP19 and OsHIPP20 (**Fig. 5**) consistent with the view that these stealthy effectors have retained their virulence activities. This demonstrates that effector variation can affect the phenotypic outcomes of disease susceptibility and

resistance independently through mediating bespoke interactions with different HMA domains. This elegant model highlights a surprisingly intimate relationship between plant disease susceptibility and resistance, as well as pathogen virulence and avirulence activities, driven by complex coevolutionary dynamics between pathogen and host.

Materials and Methods

Construction of the maximum likelihood tree of HMA family genes

The protein sequences of the HMA domains were aligned by MAFFT (Katoh et al. 2013) with the following method parameter set: --maxiterate 1000 --localpair. Then, the maximum likelihood tree was constructed by IQ-TREE (Nguyen et al. 2015) with 1,000 bootstrap replicates (Hoang et al. 2018). The model was automatically selected by ModelFinder (Kalyaanamoorthy et al. 2017) in IQ-TREE (Nguyen et al. 2015).

Yeast two-hybrid assay

To identify AVR-PikD–interacting proteins, signal peptide–truncated cDNA fragments of AVR-PikD were inserted into *Eco*RI and *Bam*HI sites of pGBKT7 (bait) vector (Clontech, http://www.clontech.com/) to construct AVR-PikD/pGBKT7 (Table S2, Kanzaki et al. 2012). MATCHMAKER Library Construction & Screening kit was used to construct the rice cDNA library from leaf tissues of rice cultivar Sasanishiki 4, 24 and 48 h after inoculation with *Magnaporthe oryzae* strain Sasa2 (race 037.1). Yeast strain AH109 competent cells were transformed with pGBKT7/AVR-PikD pGADT7-Rec and the rice cDNA library by using the polyethylene glycol/lithium acetate (PEG/LiAc) method, and plated on selective agar plates containing minimal medium without Trp, Leu, Ade and His, and supplemented with 20 mg/L of 5-Bromo-4-Chloro-3-indolyl a-D-galactopyranoside (X-α-gal) and 10 mM 3-amino-1,2,4-triazole (3-AT). cDNAs in the library were transferred to pGAD-Rec vector harboring GAL4 activation domain (AD) by homologous recombination in yeast cells. Positive yeast transformants were streaked onto a minimal medium agar plate without Trp and Leu and used for sequence analysis.

To examine the protein–protein interactions between sHMAs and AVR-Pia, AVR-Pii, AVR1-CO39 and AVR-Pik alleles, yeast two-hybrid assay was performed as described previously (Kanzaki et al. 2012). Bait and prey plasmid vectors were constructed as described in Table S2. Signal peptide–truncated cDNA fragments of AVRs were amplified by PCR by using primer set (Table S2) and inserted into *Eco*RI and *Bam*HI sites of pGADT7 (prey) or pGBKT7 (bait) vectors (Clontech). sHMA cDNAs were synthesized from total RNAs of rice leaves (cultivar Sasanishiki) and inserted into

pGADT7 and pGBKT7 by using *Spe*I and *Bam*HI sites as described in Table S2. In the case of sHMAs containing *Spe*I or *Bam*HI site, In-Fusion HD Cloning Kit (Takara) was utilized to construct plasmid vectors. The various combinations of bait and prey vectors were transformed into yeast strain AH109 by using the PEG/LiAc method. To detect the protein–protein interactions, ten-fold dilution series (×1, $\times 10^{-1}$, $\times 10^{-2}$) of yeast cells (×1 : OD600=1.0) were spotted onto on basal medium lacking Trp, Leu, Ade and His but containing X-α-gal (Clontech) and 10 mM 3-amino-1,2,4-triazole (3-AT). Positive signals were evaluated by blue coloration and growth of the diluted yeast. As a control, yeast growth on basal medium lacking Trp, Leu was also checked. Details of plasmids used are indicated in Table S2. To check the protein accumulation in yeast cells, each transformant was propagated in the liquid basal medium lacking Trp, Leu with gentle shaking at 30℃ overnight. Yeast cells from 10 ml medium were collected and 100 mg of yeast cells were treated with 400µl of 0.3 N NaOH for 15 min at room temperature. Resulting yeast extracts were used for western blot analysis using anti-Myc HRP-DirecT (MBL, Woburn, MA, United States) for bait proteins and anti-HA (3F10)-HRP (Roche, Switzerland) for prey proteins.

Generation of rice mutants of OsHIPPs by CRISPR/Cas9 system

Rice plants with mutated OsHIPP19, OsHIPP20 or OsHPP04 were generated using the CRISPR/Cas9system developed by Mikami et al. (2015). Primers sgRNA.OsHIPP19.1_F: gttgAAGCTGGTGGTGATGGCCTC and sgRNA.OsHIPP19.1_R: aaacGAGGCCATCACCACCAGCTT were annealed and cloned into pU6::ccdB::gRNA cloning vector by digestion with BbsI as the target sequence. The target sequence with the OsU6 promoter was replaced into the pZH::gYSA::MMCas9 vector by digestion with AscI and PacI, generating pZH::gYSA::MMCas9:: OsHIPP19.1. Binary vector, pZH::gYSA::MMCas9:: OsHIPP19.2, pZH::gYSA::MMCas9:: OsHIPP19 & 20 and pZH::gYSA::MMCas9:: OsHPP04 were constructed by the same method, details of the primers are listed in Table S2. The rice cultivar 'Sasanishiki' was used for Agrobacterium-mediated transformation following the methods of Toki et al. (2005), with a sequence mutation. Thereafter, regenerated T0 plants were sequenced and the mutation type was confirmed the mutation type by using primers listed in Table S2. T3 lines from the selected T2 plants were used for the experiments.

Rice pathogenicity assays

Rice leaf blade punch inoculations were performed using the *M. oryzae* strains Sasa2 (without AVR-Pik alleles). A conidial suspension (3×10^5 conidia mL^{-1}) was punch inoculated onto the rice leaf one month after sowing. The inoculated plants were placed in a dew chamber at 27°C for 24 h in the dark

and transferred to a growth chamber with a photoperiod of 16 h. Disease lesions were scanned 10 days post-inoculation(dpi) and the lesion size was measured using 'Image J' software (Schneider et al. 2012). The assays were repeated at least 3 times with qualitatively similar results.

Transient gene expression assay in *N. benthamiana*

For transient protein expression, *Agrobacterium tumefaciens* strain GV3101 was transformed with the relevant binary constructs (Table S2). To detect OsHIPPs protein accumulation and stability in *N. benthamiana*, several combinations of *Agrobacterium* transformants (the ratio of each transformant is 2:7:1 for HIPP : AVR (GUS) : P19; final concentration is OD_{600}=1.0) were infiltrated using a needleless syringe into leaves of 3- to 4-weeks-old *N. benthamiana* plants grown at 23℃ in a greenhouse. Two days after infiltration, leaves were collected and homogenized by using a Multi-Beads Shocker (Yasui-Kikai, Osaka, Japan) under cooling with liquid nitrogen. Then 2 ml of extraction buffer (10% glycerol, 25 mM Tris–HCl pH 7.0, 10 mM DTT, 1tablet / 50ml cOmplete™ Protease Inhibitor Cocktail [Roche]) was added to 1 mg of leaf tissues and further homogenized. After centrifugation at 20,000×g for 15 min, the supernatant was collected and the pellet was resuspended in 2 ml (the same as supernatant volume) of extraction buffer. The supernatants and pellet samples were subjected to SDS-PAGE followed by western blotting. Proteins were immunologically detected by using anti-HA (3F10)-HRP (Roche, Switzerland) or anti-Myc-tag (HRP-DirecT) (MBL, Woburn, MA, United States) antibodies. The luminescent images were detected by luminescent Image Analyzer LAS-4000 (Cytiva, Tokyo, Japan) after treatment of ChemiLumi One Super or Ultra (Nacalai Tesque, Japan).

Co-immunoprecipitaion assay

For co-immunoprecipitation assays, FLAG-tagged OsHIPPs and HA-tagged AVR-PikD binary constructs (Table S2) were transformed into *Agrobacterium tumefaciens* strain GV3101. Proteins were independently expressed in *N. benthamiana* and extracted from the leaves (approximately 150 mg) with 400 mL of extraction buffer (50 mM Tris-HCl pH 7.5 and 150 mM NaCl). Extracts were mixed and incubated at 4 ˚C for 1 h, and further incubated with Anti-DDDDK-tag (FLAG) mAb-Magnetic Agarose (MBL, Tokyo, Japan) at 4˚C for 1 h. FLAG-agarose was washed with the same buffer 3 times and bound protein was eluted with FLAG-peptide (100 mg/mL). The eluates were used for western blot analysis using anti-HA (3F10)-HRP (Roche, Switzerland) and anti-FLAG M2-HRP (SIGMA) antibodies.

Localization of OsHIPP19 and OsHIPP20

To visualize subcellular localization of OsHIPP19 and OsHIPP20, GFP tagged OsHIPP19 and OsHIPP20 were generated by Golden Gate methods (Engler et al. 2008) using MoClo Plant Parts Kit and MoClo Plant Tool Kit (Addgene, UK). OsHIPP19 and OsHIPP20 were cloned into pICH47732 with a GFP tag at the N-terminus, and GFP:OsHIPP19 and GFP:OsHIPP20 were expressed under the control of *cauliflower mosaic virus* (CaMV) 35S double promoter and a 35S terminator.

N. benthamiana leaves were harvested 2 and 3 days after agroinfiltration, and GFP fluorescence in the leaves was observed by an Olympus FluoView FV1000-D confocal laser scanning microscope (Olympus, Japan) equipped with a Multi argon laser, a HeNe(G) laser, and a 40× UPlanSApo (0.9 numerical aperture) and a 60× UPlanSFLN (0.9 numerical aperture) objective lens. Samples were mounted in water under glass coverslips and excited with an HeNe(G) laser. A DM488/543/633 diachronic mirror, SDM beam splitter, and BA560-600 emission filter were used for observation.

Acknowledgements

This work was supported by JSPS Grant 15H05779 and 20H05681 to RT, and 18K05657 to HS; a Grant from JSPS/The Royal Society Bilateral Research for the project “Retooling rice immunity for resistance against rice blast disease” (2018-2019); the UKRI Biotechnology and Biological Sciences Research Council (BBSRC) Norwich Research Park Biosciences Doctoral Training Partnership, UK [grant BB/M011216/1]; the UKRI BBSRC, UK [grants BB/P012574, BB/M02198X]; the European Research Council [ERC; proposal 743165]; the Gatsby Charitable Trust; and the John Innes Foundation.

References

Ashikawa, I., Hayashi, N., Yamane, H., Kanamori, H., Wu, J., Matsumoto, T., Ono, K., & Yano, M. Two adjacent nucleotide-binding site-leucine-rich repeat class genes are required to confer Pikm-specific rice blast resistance. *Genetics*. **180**, 2267–2276 (2008).

Askwith, C., Eide, D., Van Ho, A., Bernard, P. S., Li, L., Davis-Kaplan, S., Sipe, D. M., & Kaplan, J. The FET3 gene of S. cerevisiae encodes a multicopper oxidase required for ferrous iron uptake. *Cell*. **76**, 403–410 (1994).

Baggs, E., Dagdas, G., & Krasileva, K. V. NLR diversity, helpers and integrated domains: making sense of the NLR IDentity. *Current Opinion in Plant Biology*. **38**, 59–67 (2017).

Banci, L., Bertini, I., Ciofi-Baffoni, S., Huffman, D. L., & O'Halloran, T. V. Solution structure of the yeast copper transporter domain Ccc2a in the apo and Cu(I)-loaded states. *The Journal of Biological Chemistry*. **276**, 8415–8426 (2001).

Barth, O., Vogt, S., Uhlemann, R., Zschiesche, W., & Humbeck, K. Stress induced and nuclear localized HIPP26 from Arabidopsis thaliana interacts via its heavy metal associated domain with the drought stress related zinc finger transcription factor ATHB29. *Plant Molecular Biology*. **69**, 213–226 (2009).

Bailey, P. C., Schudoma, C., Jackson, W., Baggs, E., Dagdas, G., Haerty, W., Moscou, M. & Krasileva, K. V. Dominant integration locus drives continuous diversification of plant immune receptors with exogenous domain fusions. *Genome Biology.* **19**, 23 (2018).

Białas, A., Zess, E. K., De la Concepcion, J. C., Franceschetti, M., Pennington, H. G., Yoshida, K., Upson, J. L., Chanclud, E., Wu, C. H., Langner, T., Maqbool, A., Varden, F. A., Derevnina, L., Belhaj, K., Fujisaki, K., Saitoh, H., Terauchi, R., Banfield, M. J., & Kamoun, S. Lessons in Effector and NLR Biology of Plant-Microbe Systems. *Molecular Plant-Microbe Interactions*. **31**, 34–45 (2018).

Bull, P. C., & Cox, D. W. Wilson disease and Menkes disease: new handles on heavy-metal transport. *Trends in Genetics*. **10**, 246–252 (1994).

Cesari, S., Thilliez, G., Ribot, C., Chalvon, V., Michel, C., Jauneau, A., Rivas, S., Alaux, L., Kanzaki, H., Okuyama, Y., Morel, J. B., Fournier, E., Tharreau, D., Terauchi, R., & Kroj, T. The rice resistance protein pair RGA4/RGA5 recognizes the *Magnaporthe oryzae* effectors AVR-Pia and AVR1-CO39 by direct binding. *The Plant Cell*. **25**, 1463–1481 (2013).

Cesari, S., Bernoux, M., Moncuquet., P, Kroj., T. & Dodds, P.N. A novel conserved mechanism for plant NLR protein pairs: the "integrated decoy" hypothesis. *Frontiers in Plant Science.* **5**, 606 (2014).

Cowan, G. H., Roberts, A. G., Jones, S., Kumar, P., Kalyandurg, P. B., Gil, J. F., Savenkov, E. I., Hemsley, P. A., & Torrance, L. Potato Mop-Top Virus Co-Opts the Stress Sensor HIPP26 for Long-Distance Movement. *Plant Physiology*. **176**, 2052–2070 (2018).

De Abreu-Neto, J. B., Turchetto-Zolet, A. C., de Oliveira, L. F., Zanettini, M. H., & Margis-Pinheiro, M. Heavy metal-associated isoprenylated plant protein (HIPP): characterization of a family of proteins exclusive to plants. *The FEBS Journal*. **280**, 1604–1616 (2013).

De Guillen, K., Ortiz-Vallejo, D., Gracy, J., Fournier, E., Kroj, T., & Padilla, A. Structure Analysis Uncovers a Highly Diverse but Structurally Conserved Effector Family in Phytopathogenic Fungi. *PLoS Pathogens*. **11**, e1005228 (2015).

De la Concepcion, J. C., Franceschetti, M., Maqbool, A., Saitoh, H., Terauchi, R., Kamoun, S., & Banfield, M. J. Polymorphic residues in rice NLRs expand binding and response to effectors of the blast pathogen. *Nature Plants*. **4**, 576–585 (2018).

De la Concepcion, J. C., Franceschetti, M., MacLean, D., Terauchi, R., Kamoun, S., & Banfield, M. J. Protein engineering expands the effector recognition profile of a rice NLR immune receptor. *eLife*. **8**, e47713 (2019).

Dykema, P. E., Sipes, P. R., Marie, A., Biermann, B. J., Crowell, D. N., & Randall, S. K. A new class of proteins capable of binding transition metals. *Plant Molecular Biology*. **41**, 139–150 (1999).

Engler, C., Kandzia, R., & Marillonnet, S. A one pot, one step, precision cloning method with high throughput capability. *PloS One*. **3**, e3647 (2008).

Fukuoka, S., Saka, N., Koga, H., Ono, K., Shimizu, T., Ebana, K., Hayashi, N., Takahashi, A., Hirochika, H., Okuno, K., & Yano, M. Loss of function of a proline-containing protein confers durable disease resistance in rice. *Science*. **325**, 998–1001 (2009).

Gao, W., Xiao, S., Li, H. Y., Tsao, S. W., & Chye, M. L. *Arabidopsis thaliana* acyl-CoA-binding protein ACBP2 interacts with heavy-metal-binding farnesylated protein AtFP6. *The New Phytologist*. **181**, 89–102 (2009).

Grund, E., Tremousaygue, D. & Deslandes, L. Plant NLRs with integrated domains: Unity makes strength. *Plant Physiology*. **179**, 1227–1235 (2020).

Guo, L., Cesari, S., de Guillen, K., Chalvon, V., Mammri, L., Ma, M., Meusnier, I., Bonnot, F., Padilla, A., Peng, Y. L., Liu, J., & Kroj, T. Specific recognition of two MAX effectors by integrated HMA domains in plant immune receptors involves distinct binding surfaces. *Proceedings of the National Academy of Sciences of the United States of America*. **115**, 11637–11642 (2018).

Hoang, D. T., Chernomor, O., von Haeseler, A., Minh, B. Q., & Vinh, L. S. UFBoot2: Improving the Ultrafast Bootstrap Approximation. *Molecular Biology and Evolution*. **35**, 518–522 (2018).

Himelblau, E., Mira, H., Lin, S. J., Culotta, V. C., Penarrubia, L. &Amasino, R. M. Identification of a functional homolog of the yeast copper homeostasis gene *ATX1* from Arabidopsis. *Plant Physiology*. **117**, 1227–1234 (1998).

Hogenhout, S. A., Van der Hoorn, R. A., Terauchi, R. & Kamoun, S. Emerging concepts in effector biology of plant-associated organisms. *Molecular Plant-Microbe Interactions*. **22**, 115–122 (2009).

Imran, Q. M., Falak, N., Hussain, A., Mun, B. G., Sharma, A., Lee, S. U., Kim, K. M., & Yun, B. W. Nitric Oxide Responsive Heavy Metal-Associated Gene *AtHMAD1* Contributes to Development and Disease Resistance in *Arabidopsis thaliana*. *Frontiers in Plant Science*. **7**, 1712 (2016).

Kalyaanamoorthy, S., Minh, B. Q., Wong, T., von Haeseler, A., & Jermiin, L. S. ModelFinder: fast model selection for accurate phylogenetic estimates. *Nature Methods*. **14**, 587–589 (2017).

Kanzaki, H., Yoshida, K., Saitoh, H., Fujisaki, K., Hirabuchi, A., Alaux, L., Fournier, E., Tharreau, D., & Terauchi, R. Arms race co-evolution of *Magnaporthe oryzae AVR-Pik* and rice *Pik* genes driven by their physical interactions. *The Plant Journal*. **72**, 894–907 (2012).

Katoh, K., & Standley, D. M. MAFFT multiple sequence alignment software version 7: improvements in performance and usability. *Molecular Biology and Evolution*. **30**, 772–780 (2013).

Kawahara, Y., de la Bastide, M., Hamilton, J. P., Kanamori, H., McCombie, W. R., Ouyang, S., Schwartz, D. C., Tanaka, T., Wu, J., Zhou, S., Childs, K. L., Davidson, R. M., Lin, H., Quesada-Ocampo, L., Vaillancourt, B., Sakai, H., Lee, S. S., Kim, J., Numa, H., Itoh, T., … Matsumoto, T. Improvement of the *Oryza sativa* Nipponbare reference genome using next generation sequence and optical map data. *Rice*. **6**, 4 (2013).

Kroj, T., Chanclud, E., Michel-Romiti, C., Grand, X., Morel, J.-B. Integration of decoy domains derived from protein targets of pathogen effectors into plant immune receptors is widespread. *New Phytologist.* **210**, 618–626 (2016).

Le Roux, C., Huet, G., Jauneau, A., Camborde, L., Tremousaygue, D., Kraut, A., Zhou, B., Levaillant, M., Adachi, H., Yoshioka, H., Raffaele, S., Berthome, R., Coute, Y., Parker, J. E. & Deslandes, L. A receptor pair with an integrated decoy converts pathogen disabling of transcription factors to immunity. *Cell*. **161**, 1074–1088 (2015).

Maidment, J. H. R., Franceschetti, M., Maqbool, A., Saitoh, H., Jantasuriyarat, C., Kamoun, S., Terauchi, R., & Banfield, M. J. Multiple variants of the blast fungus effector AVR-Pik bind the HMA domain of the rice protein OsHIPP19 with high affinity. submitted to *bioRxiv* (2020).

Maqbool, A., Saitoh, H., Franceschetti, M., Stevenson, C. E., Uemura, A., Kanzaki, H., Kamoun, S., Terauchi, R., & Banfield, M. J. Structural basis of pathogen recognition by an integrated HMA domain in a plant NLR immune receptor. *eLife*. **4**, e08709 (2015).

Mikami, M., Toki, S., & Endo, M. Comparison of CRISPR/Cas9 expression constructs for efficient targeted mutagenesis in rice. *Plant Molecular Biology*. **88**, 561–572 (2015).

Nguyen, L. T., Schmidt, H. A., von Haeseler, A., & Minh, B. Q. IQ-TREE: a fast and effective stochastic algorithm for estimating maximum-likelihood phylogenies. *Molecular Biology and Evolution*. **32**, 268–274 (2015).

Okuyama, Y., Kanzaki, H., Abe, A., Yoshida, K., Tamiru, M., Saitoh, H., Fujibe, T., Matsumura, H., Shenton, M., Galam, D. C., Undan, J., Ito, A., Sone, T., & Terauchi, R. A multifaceted genomics approach allows the isolation of the rice Pia-blast resistance gene consisting of two adjacent NBS-LRR protein genes. *The Plant Journal*. **66**, 467–479 (2011).

Pufahl, R. A., Singer, C. P., Peariso, K. L., Lin, S. J., Schmidt, P. J., Fahrni, C. J., Culotta, V. C., Penner-Hahn, J. E., & O'Halloran, T. V. Metal ion chaperone function of the soluble Cu(I) receptor Atx1. *Science*. **278**, 853–856 (1997).

Puig, S., Mira, H., Dorcey, E., Sancenon, V., Andres-Colas, N., Garcia-Milina, A., Burkhead, J. L., Gogolin, K. A., Abdel-Ghany, S. E., Thiele, D. J., Ecker, J. R., Pilon, M. & Penarrubia, L. Higher plants possess two different types of ATX1-like copper chaperones. *Biochem Biophys Res Commun.* **354**, 385–390 (2007).

Rodakovic, Z., Anjam, M. S., Escobar, E., Chopra, D., Cabrera, J., Silva, A. C., Escobar, C., Sobczak, M., Grundier, F. M. W. & Siddique, S. Arabidopsis *HIPP27* is a host susceptibility gene for the beet cyst nematode *Heterodera shachtii*. *Molecular Plant Pathology*. **19**, 1917–1928 (2018).

Rosenzweig, A. C., & O'Halloran, T. V. Structure and chemistry of the copper chaperone proteins. *Current Opinion in Chemical Biology*. **4**, 140–147 (2000).

Sarris, P. F., Duxbury, Z., Huh, S. U., Ma, Y., Segonzac, C., Sklenar, J., Derbyshire, P., Cevik, V., Rallapalli, G., Saucet, S. B., Wirthmueller, L., Menke, F. L. H., Sohn, K. H. & Jones, J. D. G. A plant immune receptor detects pathogen effectors that target WRKY transcription factors. *Cell.* **161**, 1089–1100 (2015).

Sarris, P. F., Cevik, V., Dagdas, G., Jones, J.D. & Krasileva K.V. Comparative analysis of plant immune receptor architectures uncovers host proteins likely targeted by pathogens. *BMC Biol*ogy. **14**, 8 (2016).

Schneider, C. A., Rasband, W. S., & Eliceiri, K. W. NIH Image to ImageJ: 25 years of image analysis. *Nature methods*. **9**, 671–675 (2012).

Shi, N.N., Ruan, H.C., Liu, X.Z., Yang, X.J., Dai, Y.L., Gan, L., Chen, F.R. & Du, Y.X. Virulence structure of *Magnaporthe oryzae* populations from Fujian Province, China. *Canadian J. Plant Patholology*. **40**, 542–550 (2018).

Shin, L.J., Lo, J.C. & Yeh, K.C. Copper chaperone antioxidant protein 1 is essential for copper homeostasis. *Plant Physiology*. **159**, 1099–1110 (2012).

Toki, S., Hara, N., Ono, K., Onodera, H., Tagiri, A., Oka, S., & Tanaka, H. Early infection of scutellum tissue with Agrobacterium allows high-speed transformation of rice. *The Plant Journal*. **47**, 969–976 (2006).

Wu, C.H., Krasileva, K.V., Banfield, M.J., Terauchi, R. & Kamoun, S. The "sensor domains" of plant NLR proteins: more than decoys? *Frontiers in Plant Science.* **6**, 134 (2015).

Yoshida, K., Saitoh, H., Fujisawa, S., Kanzaki, H., Matsumura, H., Yoshida, K., Tosa, Y., Chuma, I., Takano, Y., Win, J., Kamoun, S., & Terauchi, R. Association genetics reveals three novel avirulence genes from the rice blast fungal pathogen *Magnaporthe oryzae*. *The Plant Cell*. **21**, 1573–1591 (2009).

Zhang, X., Feng, H., Feng, C., Xu, H., Huang, X., Wang, Q., Duan, X., Wang, X., Wei, G., Huang, L., & Kang, Z. Isolation and characterisation of cDNA encoding a wheat heavy metal-associated isoprenylated protein involved in stress responses. *Plant Biology*. **17**, 1176–1186 (2015).

Zhu, Y., Liu, L., Shen, L., & Yu, H. NaKR1 regulates long-distance movement of FLOWERING LOCUS T in *Arabidopsis*. *Nature Plants*. **2**, 16075 (2016).

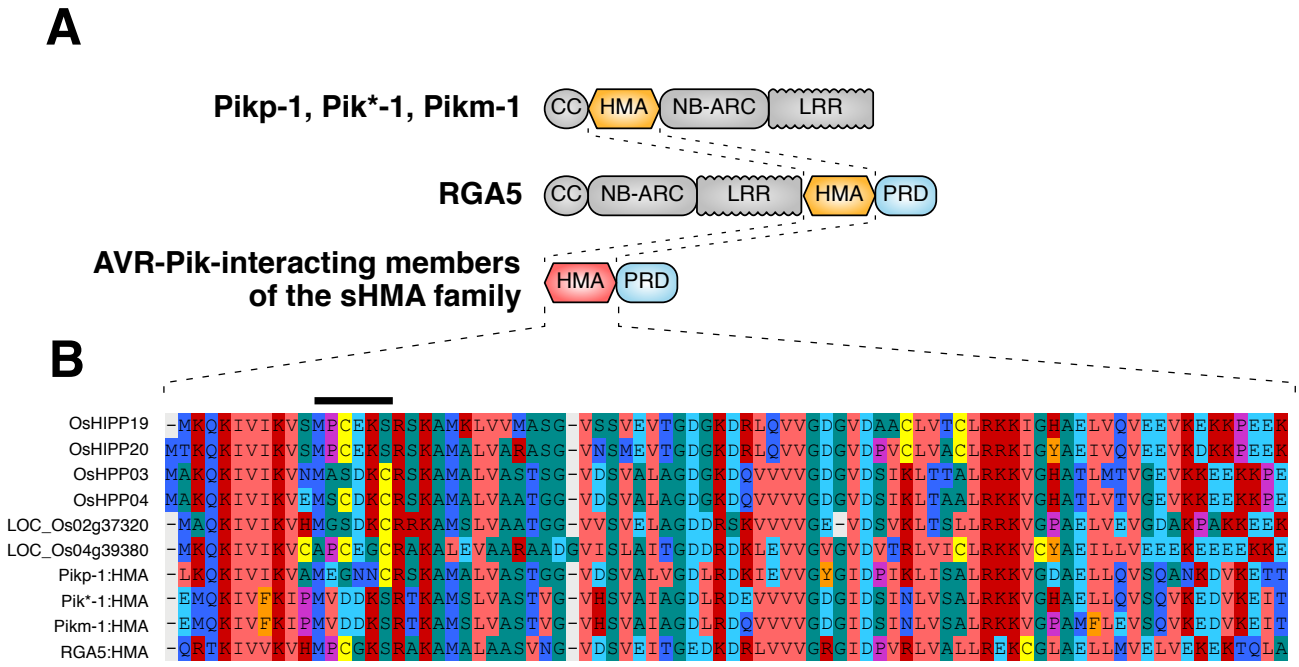

Fig. 1. Architecture of a subset of HMA domain containing proteins of rice.
(**A**) Schematic representation of the Pik-1 (Pikp-1, Pik*-1, Pikm-1) and RGA5 Nucleotide-binding Leucine Rich Repeat Receptors (NLRs) and small HMA (sHMA) proteins of rice. CC: coiled-coil domain; NB-ARC: nucleotide-binding domain; LRR: Leucine Rich Repeat; PRD: Proline-rich domain. (**B**) Amino acid sequence alignment of a subset of HMA proteins of rice. The black bar highlights the putative metal-binding motif MxCxxC.

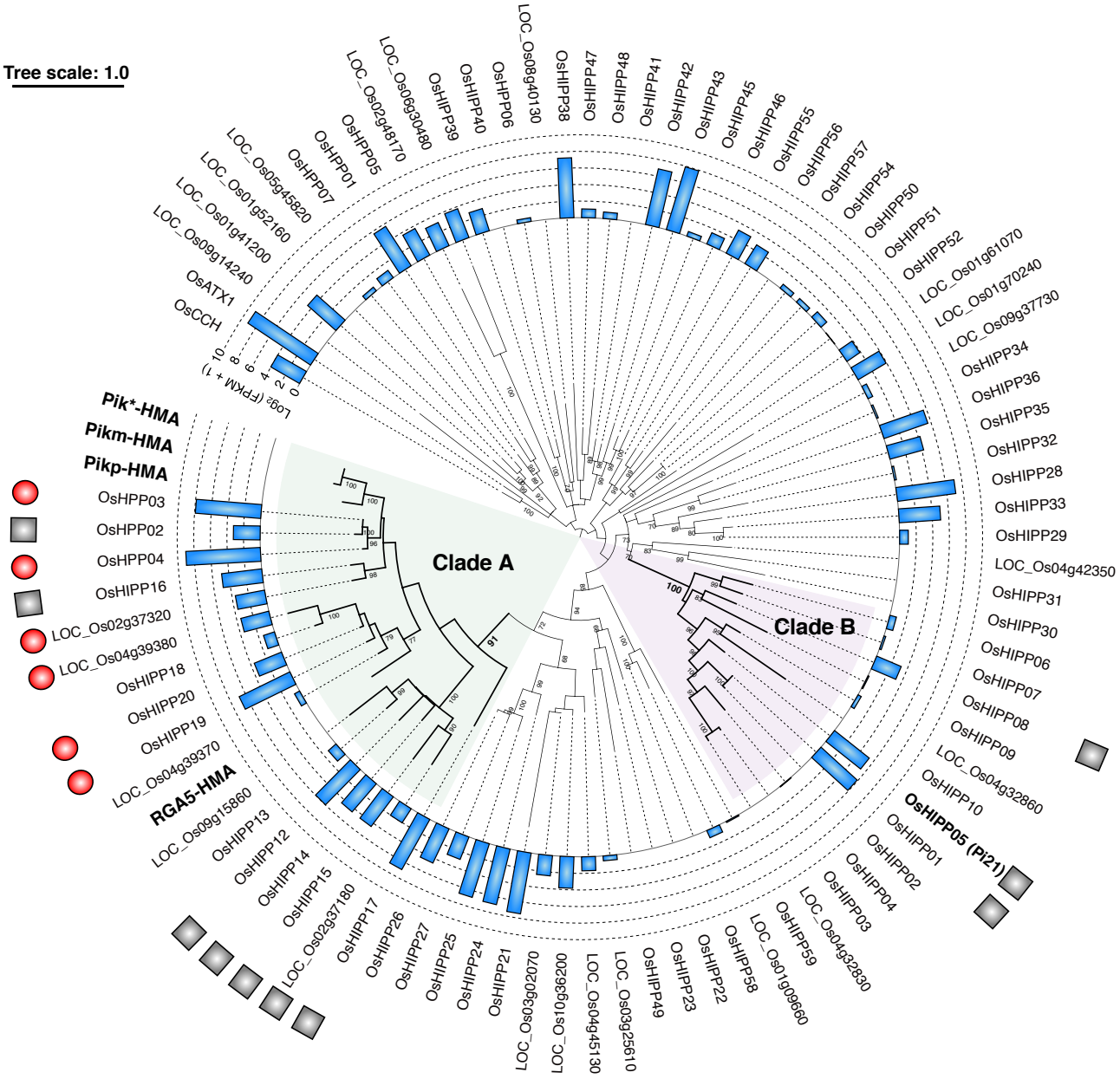

Fig. 2. AVR-PikD binds Clade A sHMAs. A maximum likelihood tree of the HMA domains of 87 sHMA of rice (center circle). Amino acid sequences of the HMA domains were aligned and used for construction of the phylogenetic tree. The numbers on the branches indicate bootstrap values after 1,000 replications. Expression levels of the genes are shown by blue bars (log_2(FPKM+1) value; middle circle). Results of yeast 2-hybrid (Y2H) interactions between AVR-PikD and sHMA in the two clades (Clade A and B) are indicated in the outer circle (red dots: binding; gray square: no binding). Note Pi21 (OsHIPP05) belongs to Clade B.

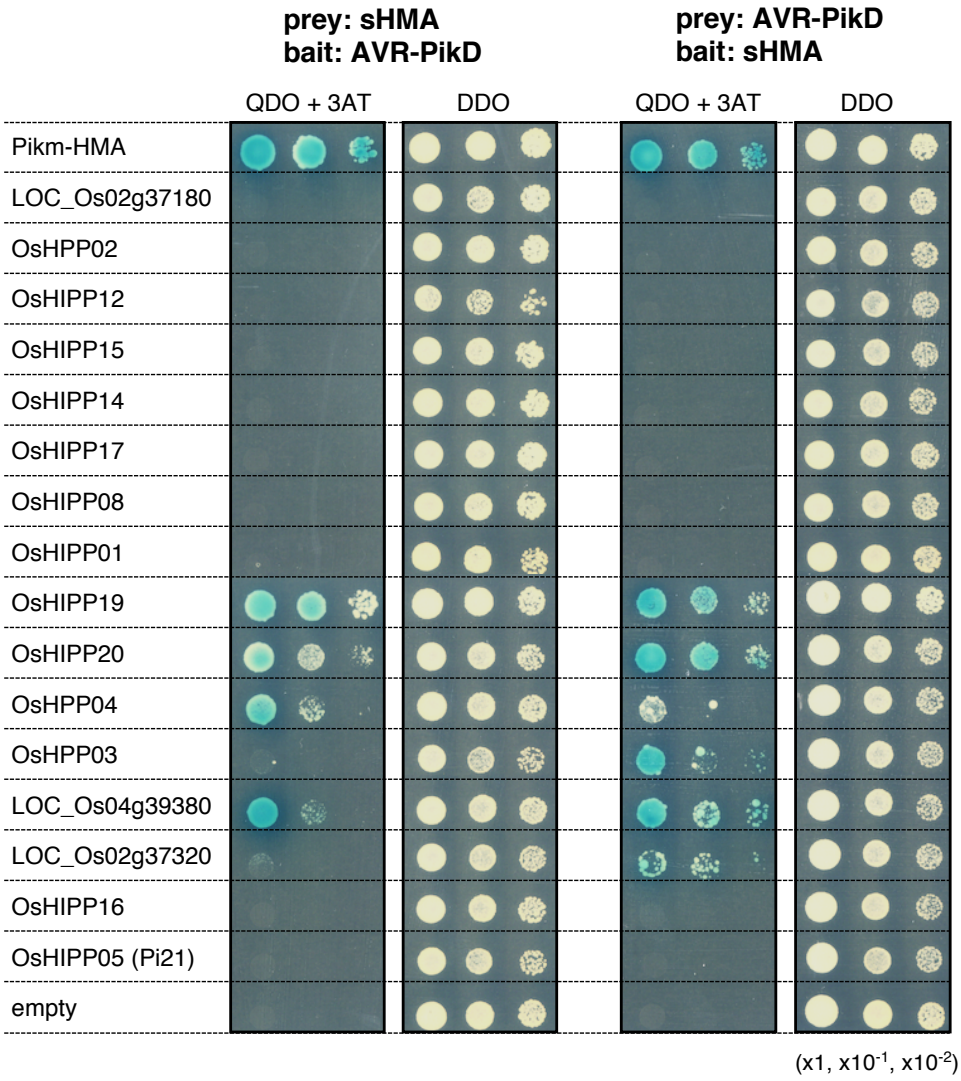

Fig. 3. AVR-PikD interacts with Clade A sHMA proteins in yeast 2-hybrid assay (Y2H).

Interactions between AVR-PikD and a subset of sHMA proteins were tested by Y2H. sHMA proteins were used as prey and AVR-PikD as bait (left panels) and AVR-PikD was used as prey and sHMA proteins as bait (right panels). Results of high stringency selection (QDO+3AT: $Trp^{-}Leu^{-}Ade^{-}His^{-}$ Xα gal^{+},10 mM 3AT) as well as no selection (DDO) are shown.

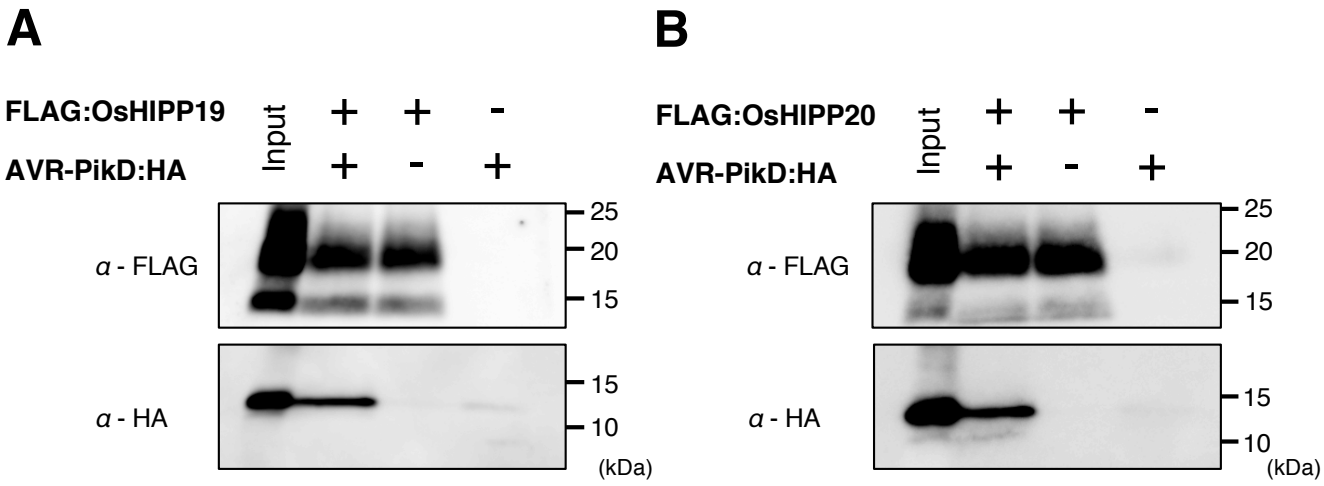

Fig. 4. Co-immunoprecipitation shows AVR-PikD binds OsHIPP19 and OsHIPP20.
(**A**) Binding assay between OsHIPP19 and AVR-PikD. (**B**) Binding assay between OsHIPP20 and AVR-PikD. Epitope-tagged proteins, AVR-PikD:HA, FLAG:OsHIPP19 and FLAG:OsHIPP20, were separately expressed in *Nicotiana benthamiana* leaves and the leaf extracts were mixed in vitro. The protein mixture was applied to an anti-FLAG antibody column and the bound proteins were detected by an anti-FLAG antibody (top) and an anti-HA antibody (bottom).

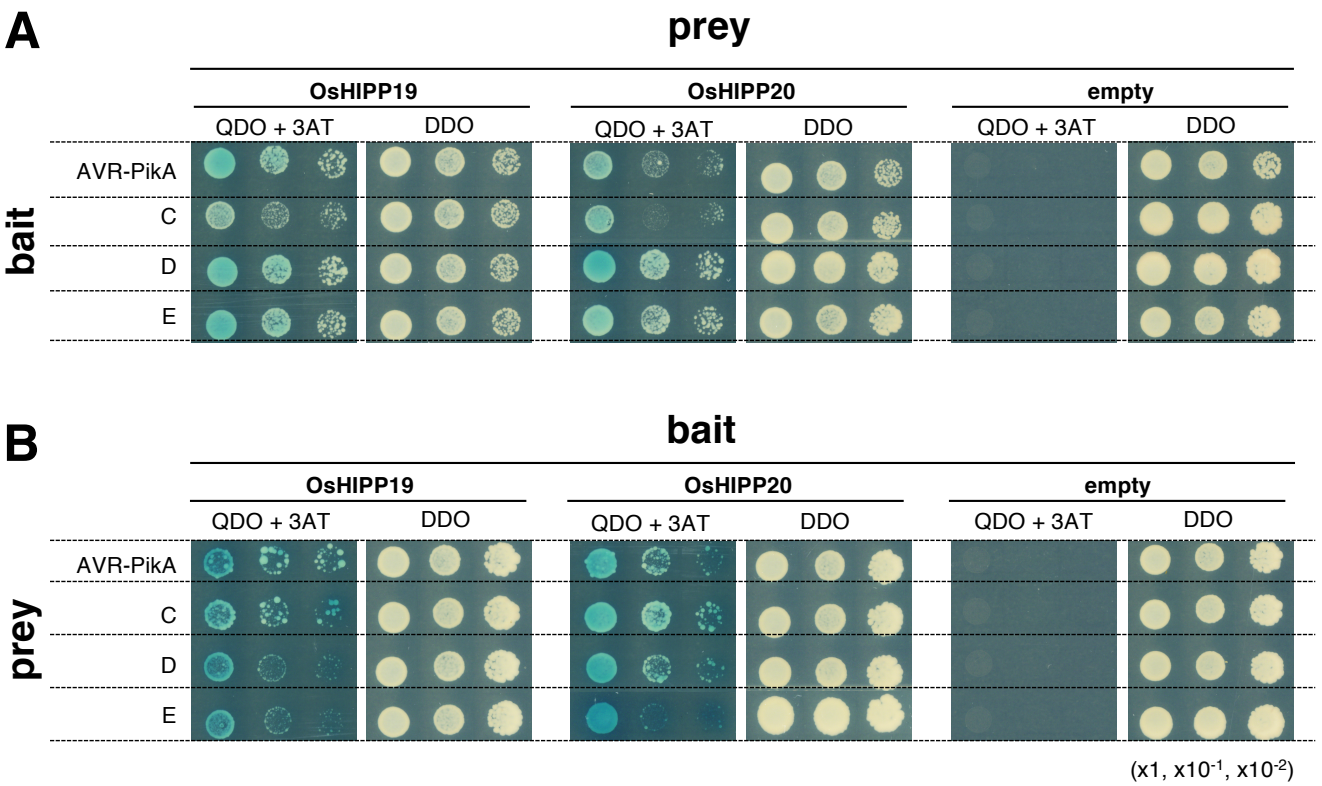

Fig. 5. All tested AVR-Pik variants (A, C, D and E) bind OsHIPP19 and OsHIPP20.
(**A**) AVR-Pik allelic variants (A, C, D and E) were used as bait and OsHIPP19 and OsHIPP20 used as prey. (**B**) AVR-Pik allelic variants were used as prey and OsHIPP19 and OsHIPP20 used as bait (bottom) . Results with empty vector indicate no autoactivation with effector constructs. Results of high stringency selection (QDO+3AT: $Trp^{-}Leu^{-}Ade^{-}His^{-}$ Xα gal^{+},10 mM 3AT) as well as no selection (DDO) are shown.

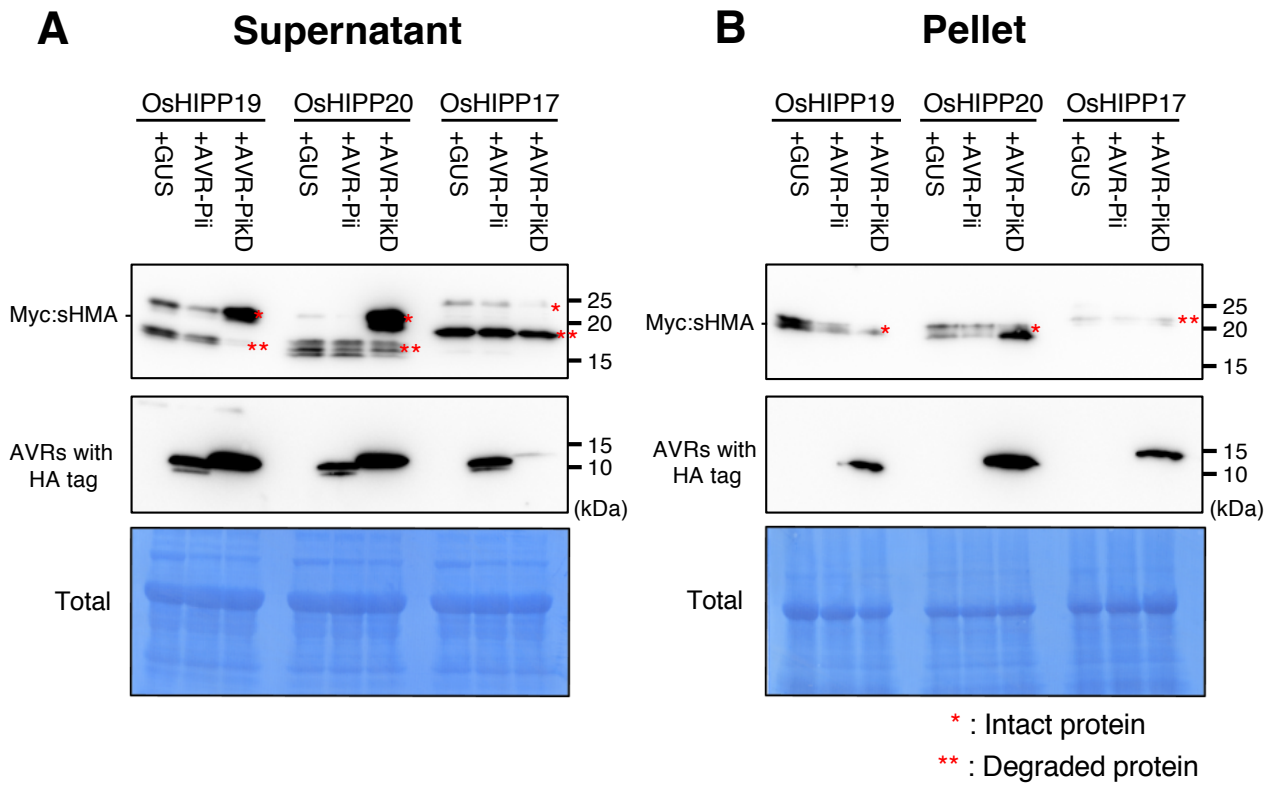

Fig. 6. AVR-PikD stabilizes sHMA proteins in planta.
sHMA proteins (Myc:OsHIPP19, Myc:OsHIPP20 and Myc:OsHIPP17) were transiently expressed in *N. benthamiana* leaves together with either GUS, HA:AVR-Pii or AVR-PikD:HA and were detected by an anti-Myc antibody. The results for supernatant fraction (A) and pellet fraction (B) after fractionation of leaf extract are shown. In the supernatant fraction, OsHIPP19 and OsHIPP20 bound by AVR-PikD remain largely stable, whereas OsHIPP19 and OsHIPP20 expressed with GUS or AVR-Pii were degraded to a lower mass fragment. OsHIPP17 does not bind AVR-PikD and is degraded even in the presence of the effector. OsHIPP19 and OsHIPP20 proteins in the pellet fraction were intact irrespective of the presence or absence of AVR-PikD, whereas OsHIPP17 in the pellet was degraded to a smaller fragment. AVR-PikD seems to accumulate in the pellet fraction when it does not bind an sHMA. We obtained similar results in three independent experiments.

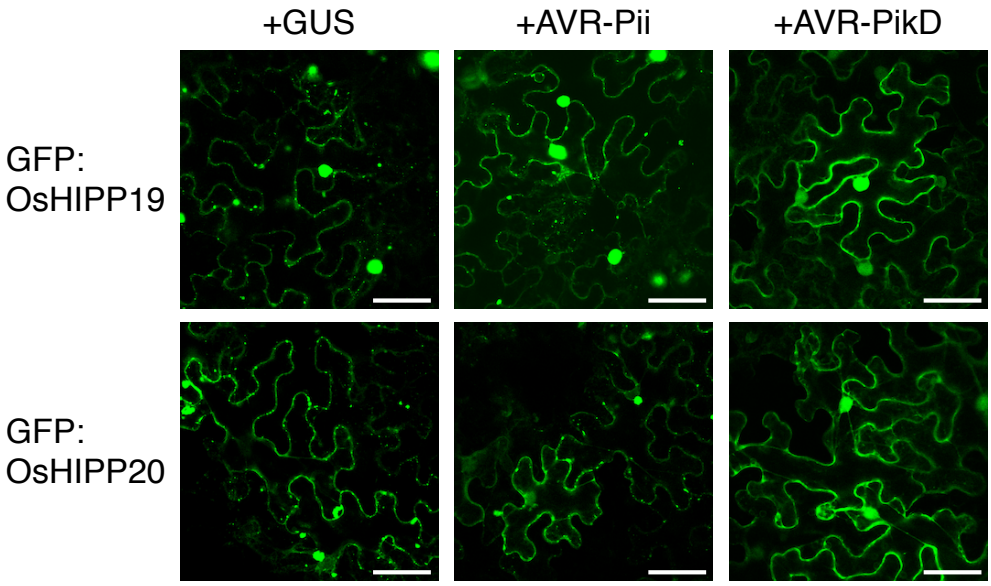

Fig. 7. AVR-PikD binding affects subcellular localization of sHMA proteins expressed in *N. benthamiana.*

OsHIPP19 (top) and OsHIPP20 (bottom) proteins fused with GFP at their N-termini (GFP:OsHIPP19 and GFP:OsHIPP20, respectively) were transiently expressed in *N. benthamiana* leaves by agroinfiltration together with GUS (left), AVR-Pii (center) or AVR-PikD (right) and were observed under confocal laser microscopy. GFP:OsHIPP19 and GFP:OsHIPP20 accumulate to punctae-like structures when expressed with GUS or AVR-Pii, whereas these proteins were evenly distributed in the cytoplasm when expressed with AVR-PikD. We obtained similar results in three independent experiments. Scale bar: 50 µm.

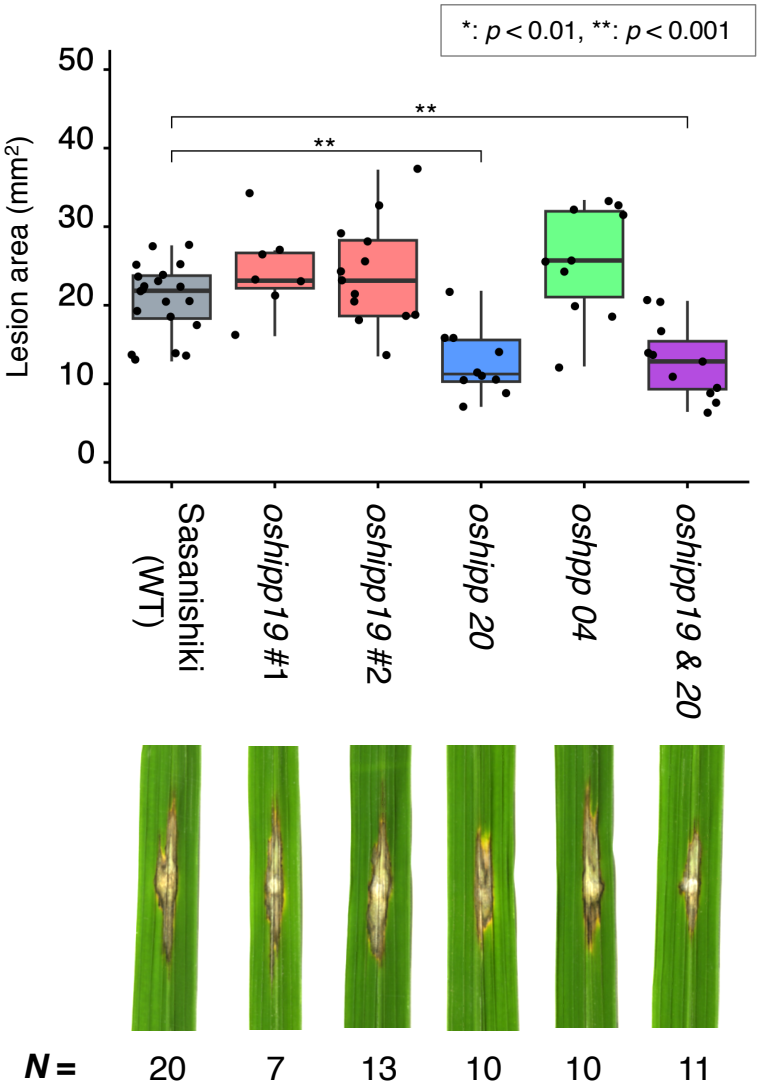

Fig. 8. *OsHIPP20* is a susceptibility gene (S-gene).
The compatible *Magnaporthe oryzae* isolate Sasa2 was punch inoculated onto the leaves of rice cultivar Sasanishiki as well as the sHMA-knockout lines of Sasanishiki (*oshipp19*#1, *oshipp19*#2, *oshiipp20*, *oshpp04* as well as *oshipp19* & *oshipp20*). Box plots show lesion area sizes in the rice lines (top). Statistical significance is shown after t-test. Photos of typical lesions developed on the leaves after inoculation of *M. oryzae* (bottom). The number of leaves used for experiments are indicated below.

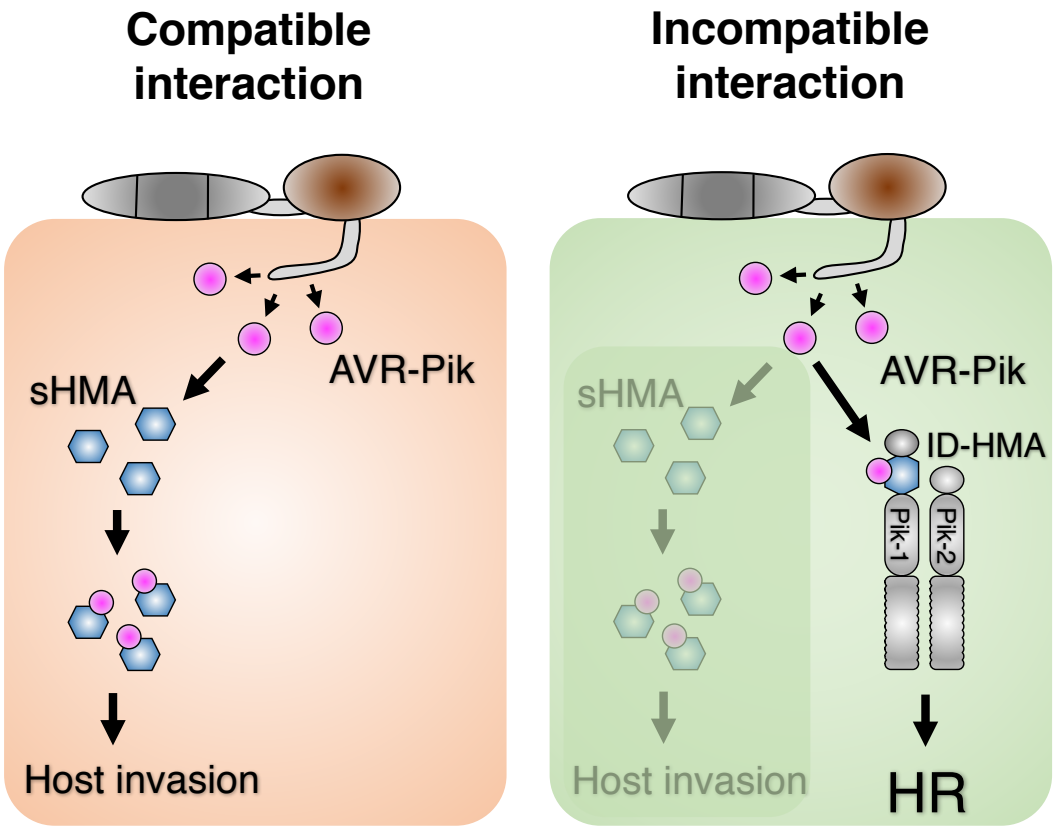

Fig. 9. Schematic representation of a model showing molecular interactions between the AVR-Pik effector, rice sHMA proteins and Pik NLRs.
In the compatible interaction (susceptible, left), AVR-Pik binds rice sHMA proteins and stabilizes them, possibly enhancing pathogen virulence. In the incompatible interaction (resistant, right), AVR-Pik interacts with integrated HMA domains of the Pik-1 NLRs which, together with Pik-2, triggers disease resistance by the hypersensitive response (HR).

Table S1. Rice proteins that interacted with AVR-PikD in the Y2H screen.
We carried out two Y2H screens (1st and 2nd) and the number of positive clones with insert sequences corresponding to the designated proteins are shown.

Protein	Gene code	1st screening		2nd screening		total	
RING finger	LOC_Os02g35329	8		8		16	
OsHIPP19	LOC_Os04g39350	1		4		5	
OsHIPP20	LOC_Os04g39010	1		2		3	
OsHPP04	LOC_Os02g37300	1	total	1	total	2	total
OsHPP03	LOC_Os02g37290	0	3	1	8	1	11
Ubiquitin	LOC_Os01g22490	7		2		9	
WRKY76	LOC_Os09g25060	5		1		6	
PR-5	LOC_Os12g38170	0		5		5	
Unknown	LOC_Os04g33390	3		2		5	

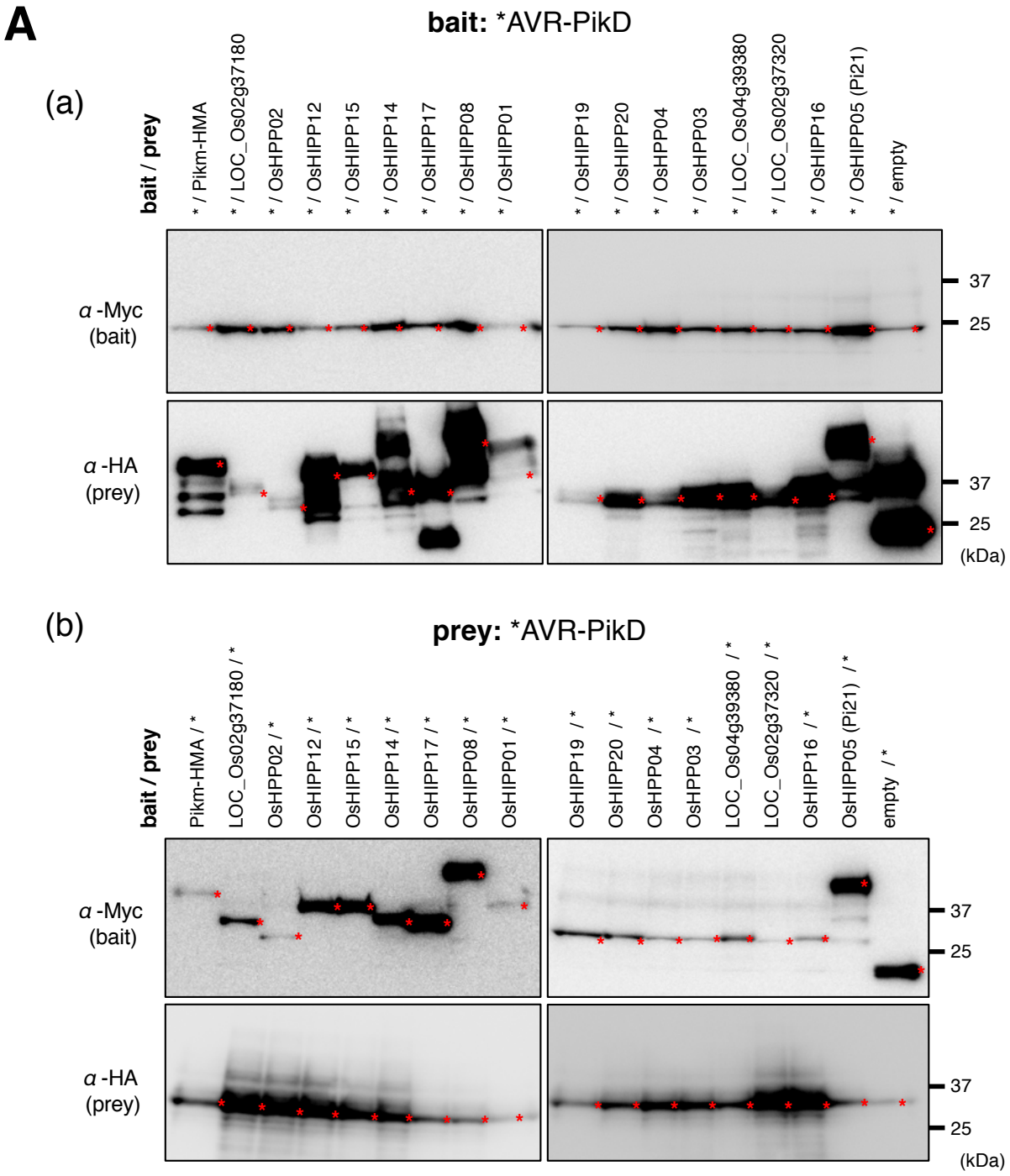

Fig. S1. A. Western blot analysis confirms protein production in the Y2H assay shown in Fig. 3.

(a) AVR-PikD was used as bait and sHMA proteins as prey. (b) AVR-PikD was used as prey and sHMA proteins as bait. The bait protein was tagged with the Myc epitope and the prey protein tagged with the HA epitope. The protein bands expressed from each vectors are marked by red asterisks. The positions of molecular size marker are indicated on the right (kDa).

B

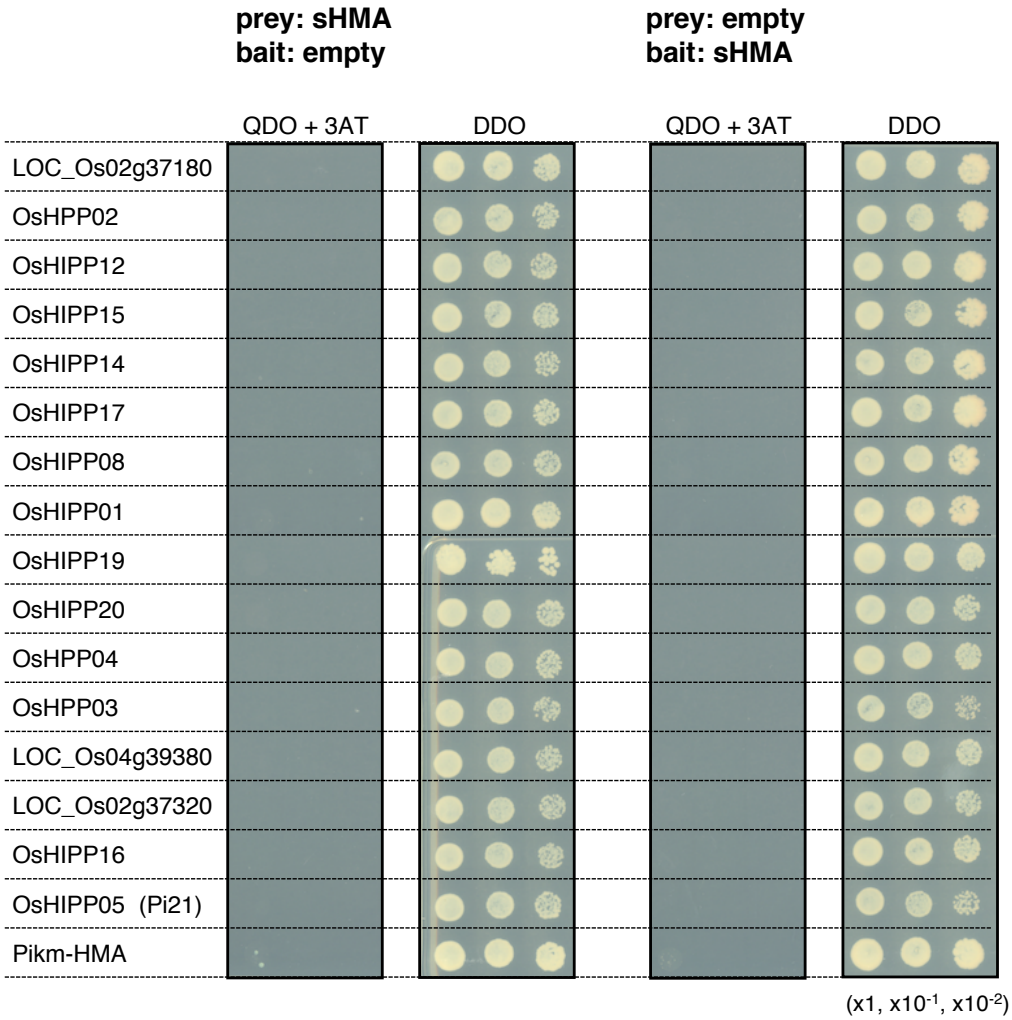

Fig. S1. B. Control Y2H experiments show no auto-activation of sHMA constructs used in Fig. 3.

sHMA proteins were used as prey (left) or bait (right). Results of high stringency selection (QDO+3AT: $Trp^-Leu^-Ade^-His^-$ Xα gal^+,10 mM 3AT) as well as no selection (DDO) are shown.

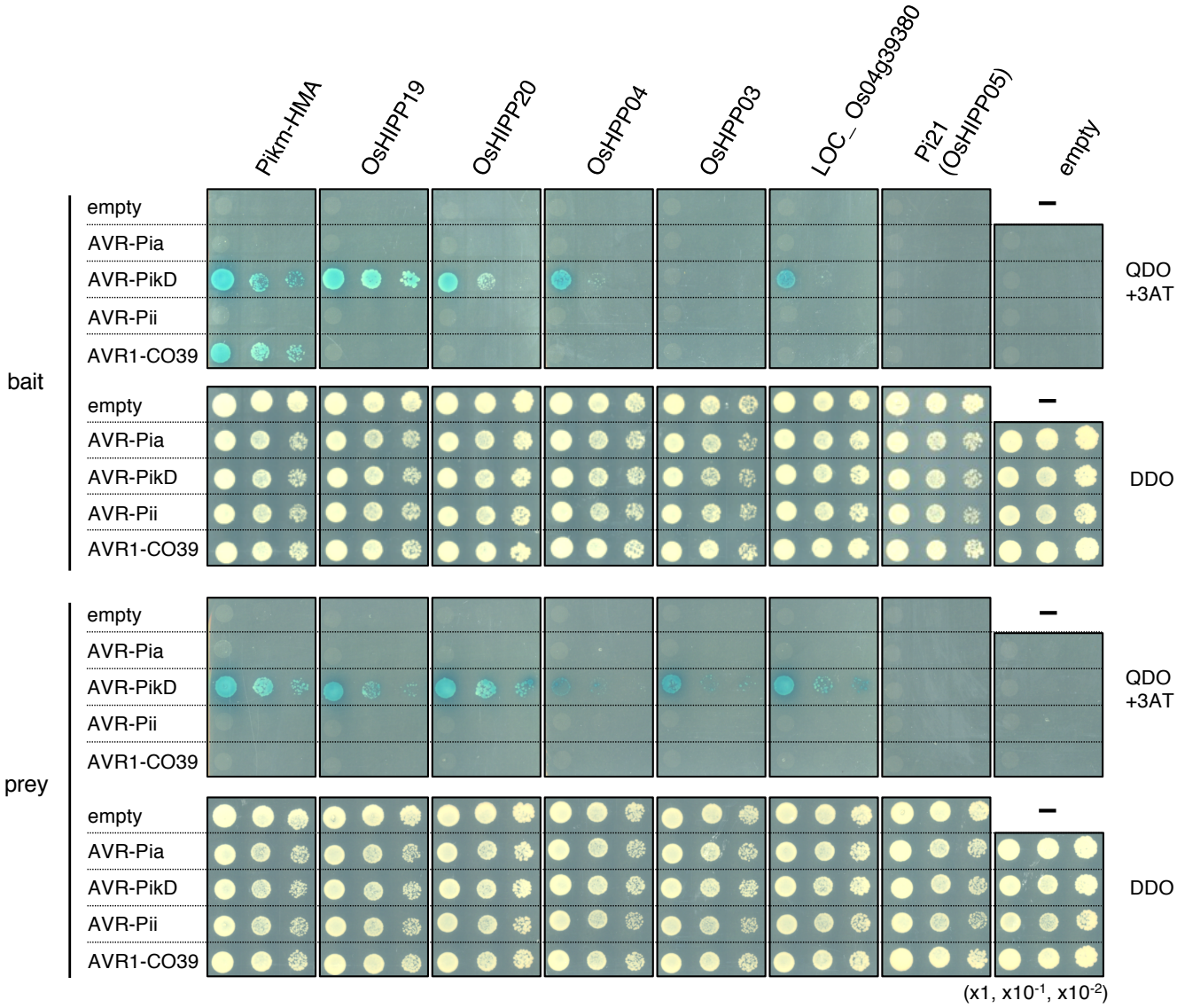

Fig. S2. AVR-Pia and AVR1-CO39 do no bind Clade A sHMAs or Pi21.
Four *Magnaporthe oryzae* effectors, AVR-Pia, AVR-PikD, AVR-Pii and AVR1-CO39 were tested for their binding with Clade A sHMAs (OsHIPP19, OsHIPP20, OsHPP04, OsHPP03 and LOC_Os04g39380) as well as Pi21 (OsHIPP05) of Clade B in Y2H assay with high stringency condition (QDO+3AT: $Trp^{-}Leu^{-}Ade^{-}His^{-}$ Xα gal^{+},10 mM 3AT) as well as no selection (DDO). The HMA domain of Pikm-1 NLR protein (Pikm-HMA) interacts with AVR-PikD (Kanzaki et al., 2012) and used as a positive control. AVR-Pii was used as a negative control. Top panels show the results when effectors were used as bait and sHMAs as prey, bottom panels show the results when effectors were used as prey and sHMAs as bait.

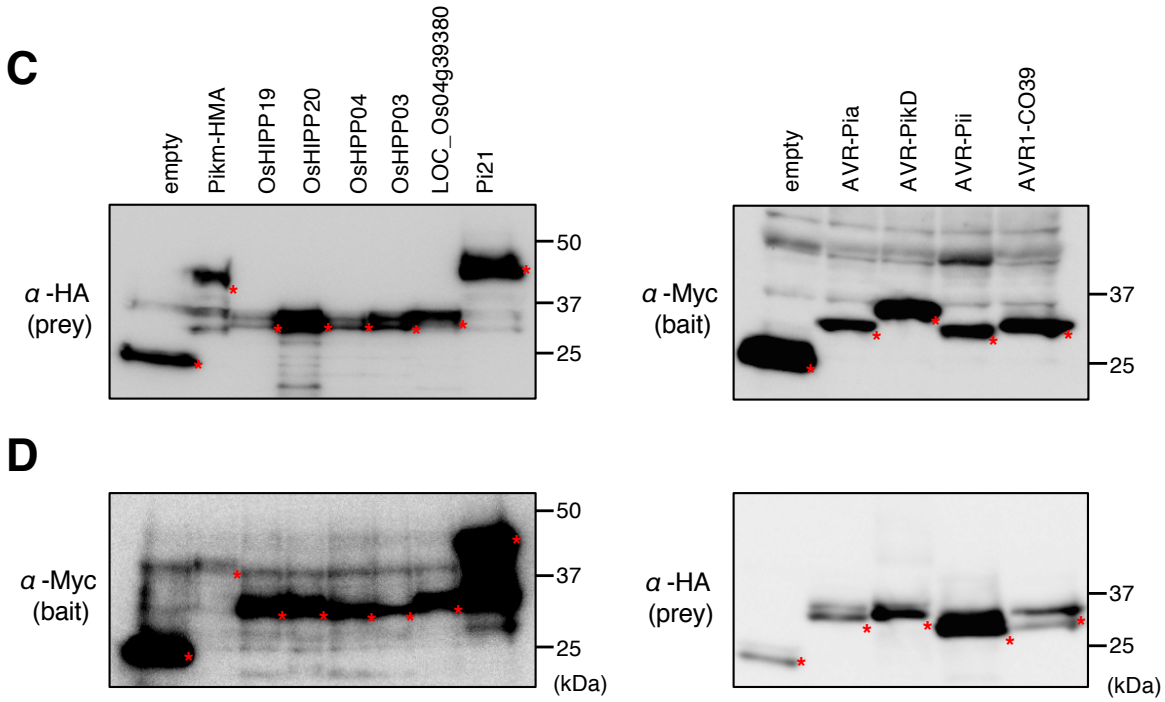

Fig. S2 continued.
Western blot analysis confirms protein production in Y2H assay as shown in Fig. S2 A, B.
(C) Western blot results corresponding to Y2H in Fig. 2A. Pikm-HMA as well as sHMAs (prey) were detected by anti-HA antibody (left panel), whereas effectors (bait) were detected by an anti-Myc antibody (right panel). (D) Western blot results corresponding to Y2H in Fig. 2B. Pikm-HMA as well as sHMAs (bait) were detected by anti-Myc antibody (left), whereas effectors (prey) were detected by an anti-HA antibody (right). The protein bands expressed from the constructs were marked by red asterisks. Molecular sizes (kDa) are indicated on the right of the panels.

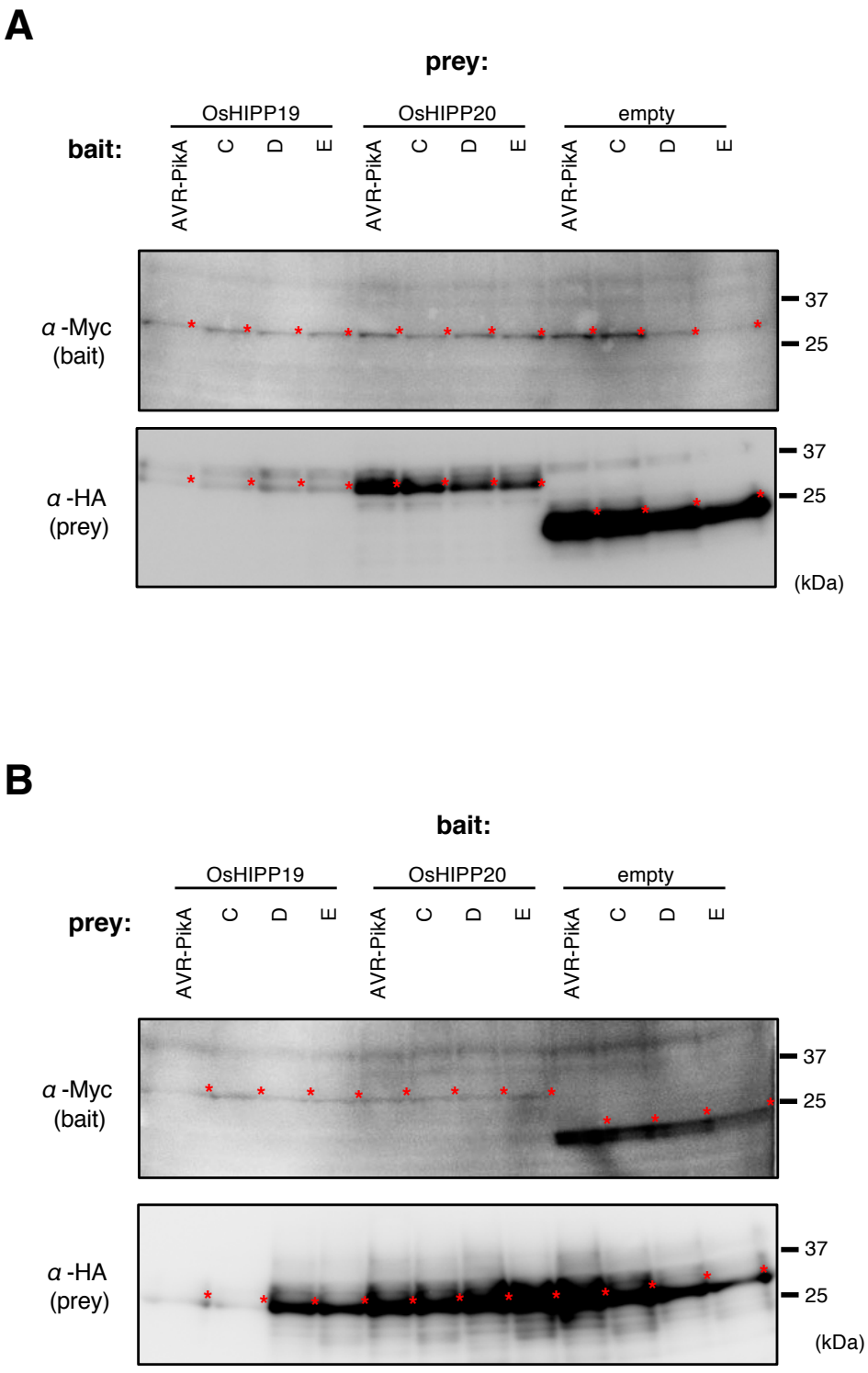

Fig. S3. Confirming the expression of AVR-Pik alleles (A, C, D and E) and OsHIPP19 and OsHIPP20 protein production in Y2H assay as shown in Fig. 4. A: sHMA proteins were used as prey and AVR-Pik alleles as bait. B: sHMA proteins were used as bait and AVR-Pik alleles as prey. Protein bands expressed from each vectors are marked with a red asterisks. The positions of molecular size marker are indicated on the right of each blot (kDa).

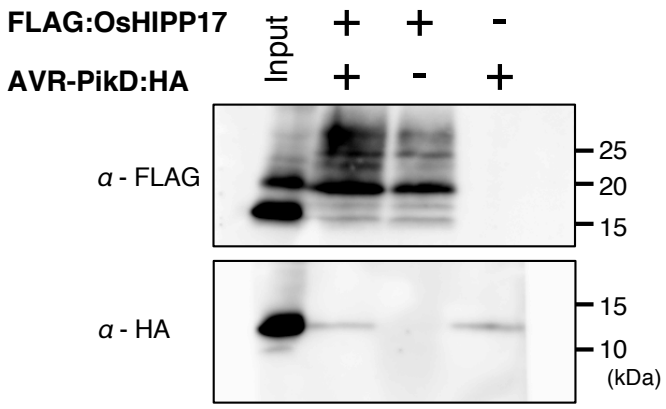

Fig. S4. Co-immunoprecipitation shows AVR-PikD does not bind OsHIPP17.
Binding assay between OsHIPP17 and AVR-PikD. Epitope-tagged proteins, AVR-PikD:HA and FLAG:OsHIPP17 were separately expressed in *Nicotiana benthamiana* leaves and the leaf extracts were mixed in vitro. The protein mixture was applied to an anti-FLAG antibody column and the bound proteins were detected by an anti-FLAG antibody (top) and an anti-HA antibody (bottom).

A

(a)

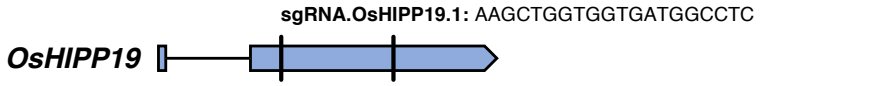

	Sequence (sgRNA.OsHIPP19.1)	Modification
WT	GCGATGAAGCTGGTGGTGATGGC-CTCCGGCGTGA	n/a
oshipp19 #1	GCGATGAAGCTGGTGGTGATGGC**A**CTCCGGCGTGA	1bp insertion

	Sequence (sgRNA.OsHIPP19.2)	Modification
WT	TACCACCACCA-CTACGGTGGGATACCGGTGGCCG	n/a
oshipp19 #2	TACCACCACCA**A**CTACGGTGGGATACCGGTGGCCG	1bp insertion

(b)

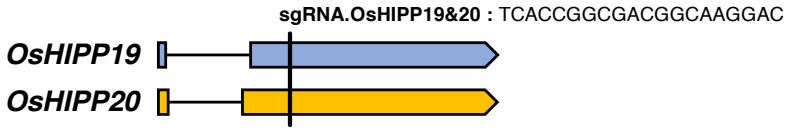

	OsHIPP19		*OsHIPP20*	
	Sequence (sgRNA.OsHIPP19&20)	Modification	Sequence (sgRNA.OsHIPP19&20)	Modification
WT	TGGAGGTCACCGGCGACGGCAAGG-ACCGGCTGCA	n/a	TGGAGGTCACCGGCGACGGCAAG-GACCGGCTGCA	n/a
oshipp20	TGGAGGTCACCGGCGACGGCAAGG-ACCGGCTGCA	n/a	TGGAGGTCACCGGCGACGGCAAGAGACCGGCTGCA	1bp(A) insertion
oshipp19 & 20	TGGAGGTCACCGGCGACGGCAAGGGACCGGCTGCA	1bp(G) insertion	TGGAGGTCACCGGCGACGGCAAAGGACCGGCTGCA	1bp(A) insertion

(c)

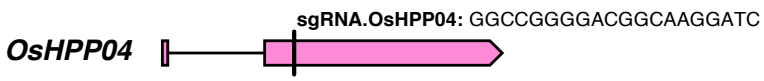

	Sequence (sgRNA.OsHPP04)	Modification
WT	GGCGCTGGCCGGGGACGGCAAGGATCAGGTGGTG	n/a
oshpp04	GGCGCTGGCCGGGGACGGCA----TCAGGTGGTG	4bps deletion

Fig. S5. A: CRISPR/Cas9-mediated knockout (KO) of sHMA genes in rice.
Guide RNA locations on the target genes as well as their sequences are shown. Tables explain nucleotide changes caused by CRISPR/Cas9 mutagenesis. (a) KO of *OsHIPP19*. (b) KO mediated by a guide RNA targeting common sequence of *OsHIPP19* and *OsHIPP20* resulted in the mutants where only *OsHIPP20* was knocked out (*oshipp20*) and both *OsHIPP19* and *OsHIPP20* were knocked out (*oshipp19&20*). (c) KO of *OsHPP04*.

B

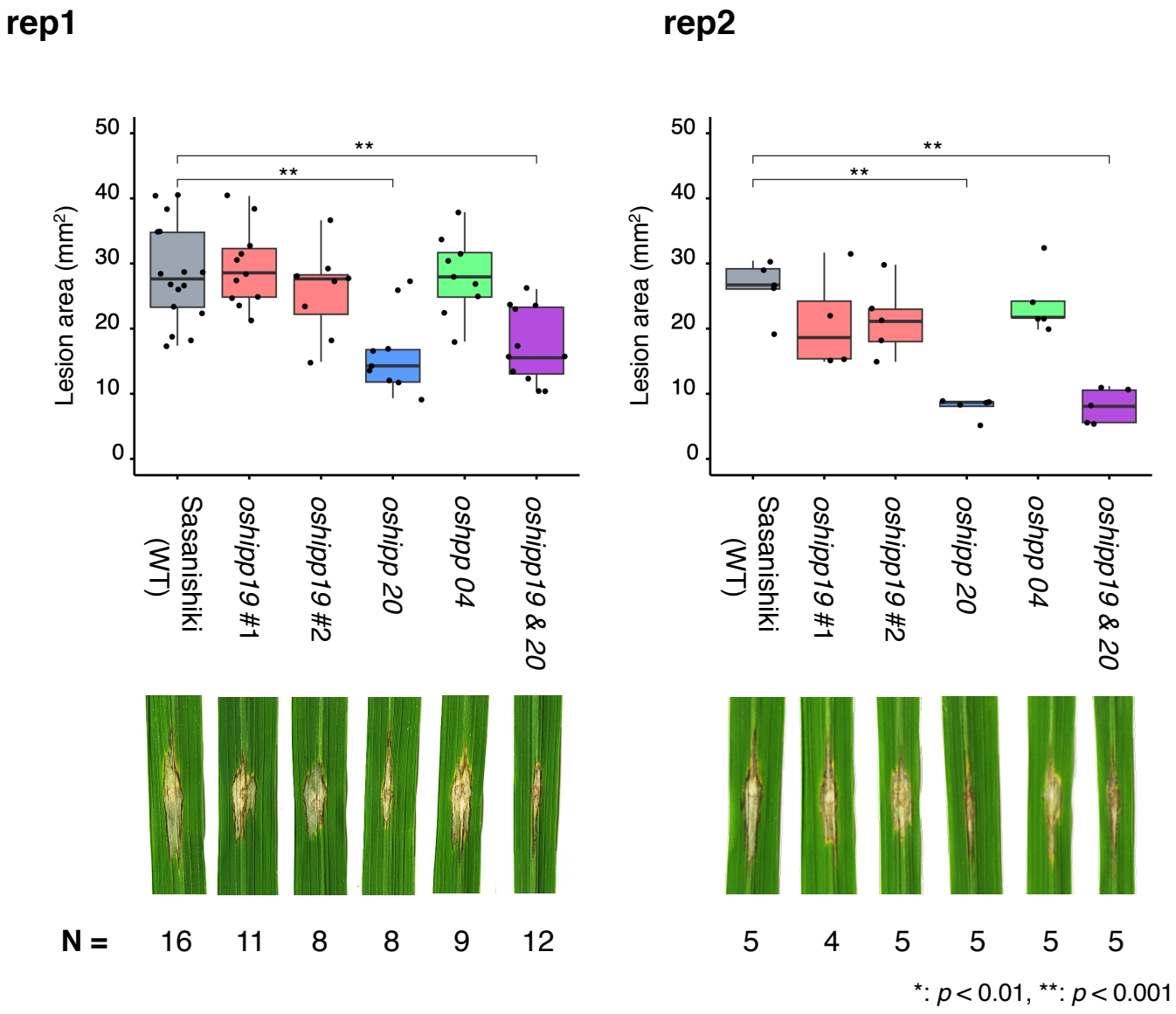

Fig. S5. B: Results of two additional inoculation experiments (rep1 and rep2) of *Magnaporthe oryzae* onto rice cultivar Sasanishiki and KO lines.
Box plots show lesion area sizes in the rice lines (top). Statistical significance is shown after t-test. Photos of typical lesions developed on the leaves after inoculation of *M. oryzae* (bottom). The number of leaves used for experiments are indicated below.